UCL Université catholique de Louvain

École polytechnique de Louvain (EPL)

epl

Stochastic geometry-based analysis of wireless communication networks

Dissertation presented by
Charles WIAME

for obtaining the Master's degree in
Electrical Engineering

Supervisors
Prof. Claude OESTGES
Prof. Luc VANDENDORPE

Readers
Prof. Jérôme LOUVEAUX
Dr. Ivan STUPIA

Academic year 2016-2017

Acknowledgements

I would like to thank several people who supported me and helped me during this academic year.

First, my supervisors, Prof. Claude Oestges and Prof. Luc Vandendorpe for their availability, advice and guidance.

Then, Prof. Jérôme Louveaux and Dr. Ivan Stupia for accepting to read this document and for dedicating time to assess my work.

I also would like to give a special thank to Mrs. Keena Armstrong for the patience she took to proofread the English of this thesis.

Last but not least, I would like to thank my family and my friends for encouraging me and supporting me all along this year.

Abstract

The objective of this master thesis is to develop an innovative framework enabling to model wireless networks and to assess their performance. This framework includes on the one hand Monte Carlo simulations and on the other hand analytical expressions derived thanks to the stochastic geometry theory. The result of this work aims at providing an optimization tool applicable to modern and future networks (e.g. relying on the 5G technology). We hence focus on three aspects that are considered to be crucial for such networks : the modeling of the propagation environment, the beamforming and the transmit power monitoring. Each of these topics is analyzed in order to gain insight into their impact on the global performance. Then, a heterogeneous network encompassing these three aspects is proposed.

L'objectif de ce travail de fin d'études est de développer un cadre novateur permettant la modélisation de réseaux cellulaires ainsi que l'évaluation de leur performance. Deux méthodes sont mises en oeuvre afin d'atteindre cet objectif. La première comprend l'utilisation de simulations de type Monte Carlo. La seconde consiste à développer des expressions analytiques au moyen de la géométrie stochastique. Les deux démarches proposées permettent d'évaluer la couverture globale du réseau en fonction de ses macroparamètres. Le résultat de ce mémoire constitue un outil d'aide à l'optimisation applicable aux réseaux modernes et futurs (notamment basés sur la 5G). Ce document est donc axé sur trois aspects considérés comme importants lors la conception de tels réseaux : la modélisation de l'environnement de propagation, le beamforming ainsi que le monitoring de la puissance d'émission. L'impact de chacune de ces thématiques sur la couverture du réseau est analysée. Pour terminer, ces trois aspects sont regroupés au sein d'un modèle de réseau hétérogène.

Contents

List of abbreviations

ASAPPP	Approximate SIR analysis based on the PPP ;
BER	Bit error rate ;
BS	Base stations ;
ccdf	Complementary cumulative distribution function ;
cdf	Cumulative distribution function ;
CLT	Central limit theorem ;
CO	Cognitive users ;
CSI	Channel state information ;
EDGE	Enhanced data rates for GSM evolution ;
HCPP	Hard core point process ;
Hetnets	Heterogeneous networks ;
LOS	Line-of-sight ;
LT	Laplace transform ;
MIMO	Multiple inputs multiple outputs ;
MPLP	Manhattan point line process ;
MRT	Maximum ratio transmission
MU-MIMO	Multi-user multiple inputs multiple outputs ;
NLOS	Non-line-of-sight ;
pdf	Probability distribution function ;
PGFL	Probability generating functional ;
PP	Point process ;
PPP	Poisson point process ;
PU	Primary users ;
QoS	Quality of service ;
rv	Random variable ;
SG	Stochastic geometry ;

SINR	Signal-to-interference-plus-noise ratio ;
SIR	Signal-to-interference ratio ;
SNR	Signal-to-noise ratio ;
UE	User equipment ;
ZF	Zero forcing.

Chapter 1

Introduction

The data rate of cellular networks has increased exponentially since the development of mobile phones. At the beginning of the century, the downlink rate of the EDGE norm (Enhanced data rates for GSM evolution) was around 384 kbit/s whilst we are now expecting up to several Gbits/s with the release of 5G. In order to achieve such a capacity, more complex, dense, and irregular networks are being deployed.

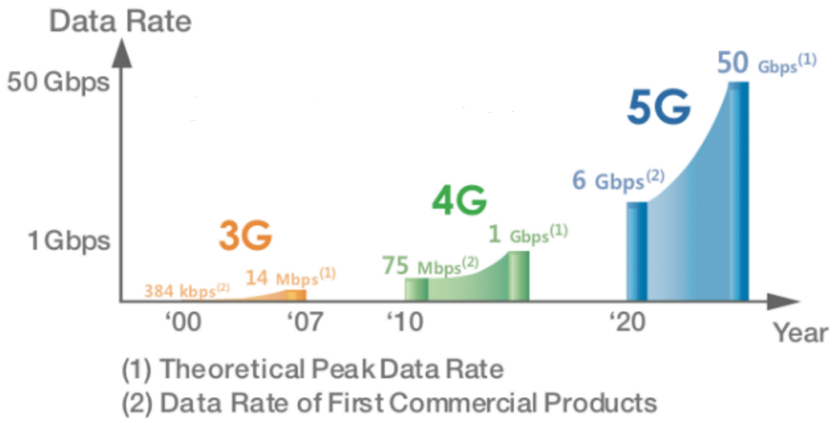

Figure 1.1: Evolution of the data rate during the past decades (Source : [Misc55])

The network models previously developed (see for instance [Misc53-Misc54]) are no longer valid due to their restrictive assumptions. To analyze modern networks, one often resorts to Monte Carlo simulations. The two main drawbacks of this option is that it is time consuming and that it does not always enable to easily gain insight. To optimize the network, it is necessary to know the impact of its macroparameters with exactitude, hence the need for analytical expressions.

Over previous years, stochastic geometry has been extensively employed to derive closed-form formulas characterising networks [SG2]. This branch of spatial statistics can abstract network nodes as point processes. These nodes represent either base stations (BSs) or user equipments (UEs). Metrics of interest (coverage, ergodic rate, etc) can then be viewed as random variables associated with these point processes. Averaging them over all the possible locations enables to derive a tractable expression of their distribution.

Stochastic geometry (SG) is now used to analyze networks of all kind. The mathematical background of this field is described in Chapter 2. In the framework of this document, we will focus successively on three hot topics : the modeling of the shadowing effects, MIMO networks and power control algorithms.

The link between a transmit BS and a receive UE is usually assumed to be affected by three factors :

- *The path loss* that represents the decrease in power density when the waves propagate in space ;
- *The fading effects* accounting for the multipath propagation of the waves ;
- *The shadowing effects* that are due to large scale obstacles obstructing the link.

Whilst the first is usually taken into account properly, the last two are often modeled inaccurately. Indeed the fading and the shadowing are often represented as exponential and lognormal random variables. The parameters of their distribution are often determined by means of empirical models. However, using independent random variables does not induce correlation between the different links. This approach is therefore not realistic, especially regarding the shadowing which is supposed to represent large scale losses (that are physically correlated). In Chapter 3, we will present a model that attempts to fill this gap. The analysis will be based on a Manhattan grid representing an urban environment and combines both penetration and diffraction losses.

Massive MIMO systems are a promising field of the 5G research [MIMO22]. Indeed, coordinating antenna arrays brings significant improvements in terms of spectrum and energy efficiency. This comes, however, at the cost of more advanced signal processing techniques and overhead due to the CSI acquisition. Chapter 4 tackles the general question : *Given a fixed transmit power and a total number of transmit antennas, how to distribute and coordinate the antennas to optimize the global coverage distribution ?* Several beamforming and clustering techniques will be studied and compared. In terms of contribution, we will provide new analytical formulas taking the power constraint into account. Furthermore, we will present interpretations enabling to gain insight into the link between the performance of the beamformers and the propagation environment.

In Chapter 5, we will detail several dynamic power allocation schemes. These algorithms are applied on the MIMO networks developed in the preceding chapter in order to further improve their performance.

The deployment of heterogeneous networks (Hetnets) will play a significant role as well towards 5G [HetNet51]. These networks consist of cells of different sizes, ranging from km^2 (macrocells) to m^2 (femtocells). These different types of cells overlap with each other in order to cover various environments (outdoors, indoors, with few or many UEs, etc). In Chapter 6, we will propose a last model representing a network consisting of three tiers (i.e. three types of cells). This model will also encompass all the aspects discussed in the rest of the thesis (urban shadowing, MIMO systems and power control).

Chapter 2

State of the art

This chapter is structured as follows. A general introduction is given about the foundations of stochastic geometry in section 2.1. Reviews of the existing literature on shadowing models (Chap. 3), MIMO systems (Chap. 4), power control algorithms (Chap. 5) and Hetnets (Chap. 6) are then detailed in sections 2.2, 2.3, 2.4 and 2.5 respectively.

2.1 Mathematical background : stochastic geometry

Stochastic geometry is a branch of statistics studying distributions of objects in measurable spaces (typically $\mathbb{R}^n$). These objects can be either points, in which case one resorts to the point process theory, or sets, that can be analyzed by means of the random shape theory.

Network nodes can be modeled as points on a two-dimensional plane and can represent for instance BSs or UEs. The analysis of a network must yield results independent of the positions of the nodes. Indeed, the UEs undergo displacement over time, and whilst the position of the BSs is usually fixed, one wishes to obtain network properties depending on other parameters than the BS locations. For these reasons, stochastic geometry is a natural framework to capture the randomness of these nodes.

Most of the results of this section are available in [SG1-SG3].

2.1.1 The point process theory

The analysis of networks often consists in deriving expressions for metrics of interest. The computation of such variables usually requires the statistical distribution of the signal-to-interference-plus-noise ratio (SINR). This ratio depends on both channel gain and on path loss between the network nodes. When defining the hypotheses of the network, it is hence necessary to select a channel model as a well as point process (PP) accounting for the topology of the nodes.

Let us first mention the most popular PPs used in the literature and in this document :

- *The homogeneous Poisson point process* (PPP) : A PP $\Phi \in \mathbb{R}^n$ of intensity λ is Poisson if the number of points in any pair of disjoint subsets of $\mathbb{R}^n$ are independent and if the number of points in a given compact set S follows a Poisson law of parameter $\lambda\nu(S)$, where $\nu(S)$ is the Lebesgue measure (i.e. volume) of S.

  To generate a PPP in a given area A, one first generates the total number of points by means of one random sample from a Poisson law (of parameter $\lambda\nu(A)$). Afterwards, the

points can be distributed within the area using samples from a uniform law.

PPPs are the most commonly used for several reasons :

- They generally lead to tractable results, partly thanks to their probability generating functional (see below);
- They have good properties : invariance (under translation and rotation), preservation (under superposition, thinning and transformation with a kernel), etc;
- Their distribution in space is natural and realistic with respect to many real networks.

- *The binomial point process* : This PP follows the same properties as the PPP except that the number of points within the entire area is constant. The number of points inside any subset follows subsequently a binomial law.
- *The hard core point process (HCPP)* : This PP is repulsive in the sense that its points are mutually separated by a minimum distance. Compared to the PPP, it enables to model scenarios in which the BSs are not likely to be close to each other. Its main drawback is its lack of tractability. This PP has been subject to much research over the previous years [SG6] - [SG7]. Soft core point processes able to model nodes with repulsion are also investigated (e.g. *the Ginibre point process* [SG8]).
- *The Poisson cluster process* : This point process is obtained by generating a PPP and by replacing the resulting points by clusters of points. This kind of PP can be very useful to model areas with high densities of users (e.g. femtocells, see Chapter 5).

These point processes are illustrated in figure 2.1.

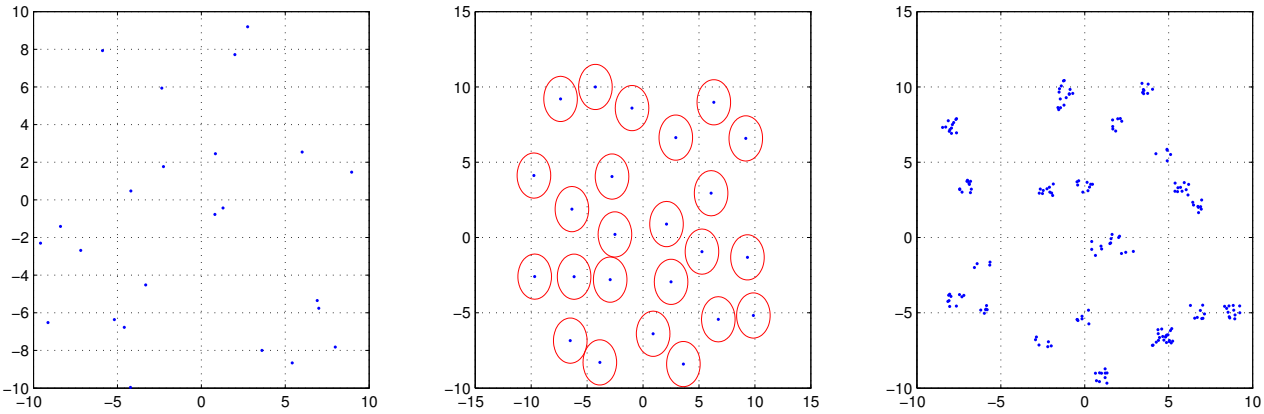

Figure 2.1: Left : PPP of intensity 1.5 generated in a square of size 20x20. Middle : HCPP of intensity 1.5 with a minimum distance of 3. Right : PCP of intensity 1.5, and whose intra cluster users are generated by means of a PPP of intensity 7 in a unit square.

Let us now state a few well-known definitions and theorems :

Any realisation of a PP can be described either thanks to the coordinates of its points X_i or by means of its random counting measure $\Psi : S \subset \mathbb{R}^n \to \mathbb{N}$. This function returns the number of points in any subset of $\mathbb{R}^n$ and can be written as $\Psi(S) = \sum_{X_i \in S} \mathbb{1}[X_i \in S]$ (where $\mathbb{1}(\cdot)$ is the indicator function). The expectation measure $\mu(S)$ is defined as the mean of the random counting measure, i.e. $\mu(S) = \mathbb{E}[\Psi(S)]$.

Let Φ a PP and $f : \mathbb{R}^n \to \mathbb{R}^+$. The probability generating functional (PGFL) of Φ with respect to function f is defined as :

$$P_\Phi(f) = \mathbb{E}\Big[\prod_{X_i \in \Phi} f(X_i)\Big]. \tag{2.1}$$

For a homogeneous PPP Φ of intensity λ, this simplifies into :

$$P_\Phi(f) = exp\Big(-\lambda \int_{\mathbb{R}^n} (1 - f(x))dx\Big). \tag{2.2}$$

The PGFL can be viewed as an equivalent for PPs of the characteristic function or moment generating function (that provide an alternative description of random variables). The PGFL enables to compute the Laplace transform (LT) of random variables of the form $F = \sum_{X_i \in \Phi} g(X_i)$. Indeed, the LT of such functions can be expressed as :

$$\mathcal{L}_F(s) = \mathbb{E}\Big[exp\Big(-s \sum_{X_i \in \Phi} g(X_i)\Big)\Big] = \mathbb{E}\Big[\prod_{X_i \in \Phi} e^{-sg(X_i)}\Big]. \tag{2.3}$$

As we will see, the form of the aggregate interference function actually corresponds to F.

Let Φ a homogeneous PPP of intensity λ and F, defined as above. Campbell's theorem states that the expectation of F can be expressed in the following way :

$$\mathbb{E}(F) = \mathbb{E}\Big[\sum_{X_i \in \Phi} f(X_i)\Big] = \int_{\mathbb{R}^n} \lambda f(x)dx. \tag{2.4}$$

Finally, Slivnyak's theorem states a PPP keeps the same distribution when removing one of its points. This result will allow to treat the interfering BSs of a given UE as a PPP (since the BS providing the useful signal is not taken into account). The interested reader will find a formal definition of this theorem in [SG5].

2.1.2 General methodology

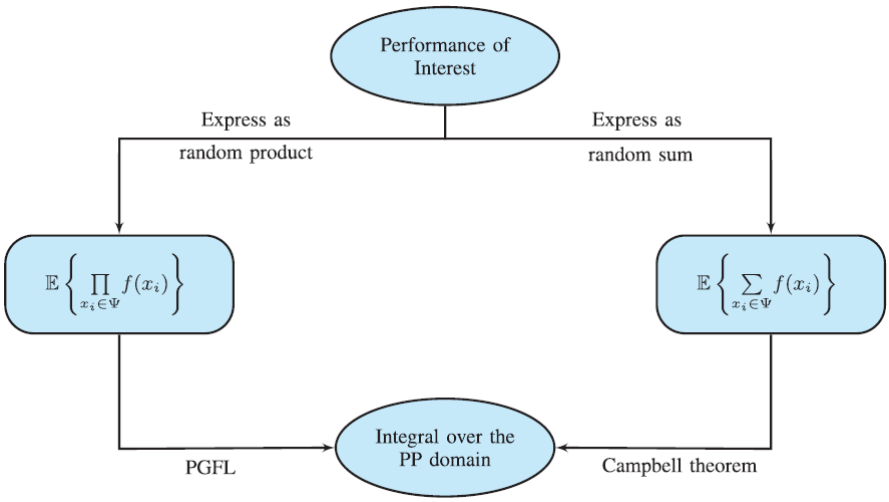

Figure 2.2: General methodology (Source : [SG3])

The procedure used by most papers to analyze networks generally follows the following steps :

- A PP is selected to model the locations of the BSs. Two distinct options are possible for the UEs. On the one hand, a second PP can be employed to distribute them. On the other hand, the analysis can sometimes be restricted to only one UE located at the origin of the network. In that case, the performance obtained at that typical user is supposed to be representative with respect to what would be measured at other user locations. In the case of Hetnets, this step might be repeated several times in order to generate the different tiers.
- A channel model is defined. Several examples are available in the next section. Regarding MIMO networks, a beamforming technique must be assigned as well.
- An analytical expression of a given performance metric is derived by averaging over all possible network realisations. As indicated on figure 2.7, the theorems stated in the previous section play an important role in this part of the analysis.

2.1.3 Performance metrics

The most studied performance metrics are listed below :

- *The outage probability* : the cumulative distribution function (cdf) of the SINR, representing the probability of the SINR to be below a given threshold. In an equivalent manner, one can define the coverage probability which is the complementary cumulative distribution function (ccdf) of the SINR.
- *The ergodic rate* : also named capacity. This metric is defined as $\mathbb{E}[\log(1 + \text{SINR}]$ and measures the mean rate averaged over all possible network realisations.
- *The symbol/bit error probability* : probability to decode a symbol/bit different from what was initially transmitted.
- *The handover rate* : rate of cell association changes.

2.1.4 The aggregate interference problem

Generally, the procedure outlined above leads to expressions involving the LT of the aggregate interference : $\mathcal{L}_{I_{agg}}(s) = \mathbb{E}[e^{-sI_{agg}}]$ or alternatively its characteristic function or moment generating function. However, the interference in general does not have a closed form probability distribution function (pdf) [SG4]. Recent developments have shown that the distribution of the interference would tend to an α-stable distribution, for which the LT and pdf are undefined [SG3]. Several techniques exist to overcome this issue :

- *Approximating the pdf* : By computing the moments of the interference and replacing them in a chosen distribution.
- *Obtaining lower/upper bounds* of the pdf : by using mathematical inequalities (Chebyshev's inequality, Chernoff bound, Markov inequality, etc). It is sometimes useful to assume dominant interferers by region or nearest n interferers.
- Using *Parseval theorem*, but this can lead to integrals that are not solvable analytically.
- Using the *Equivalent-in-Distribution approach* [SG10]. However, to the best of the author's knowledge, this method can exclusively be applied to derive the BER probability.
- Using an *ad hoc reasoning* specific to the network.

2.2 Channel models

2.2.1 Rayleigh fading

The most common model in the literature assumes Rayleigh fading on each link. Assuming a constant distance r between a transmit BS and its target UE, the received useful power at the UE can be expressed as $P_r = P_t|h|^2 r^{-\alpha}$ where α is the path loss exponent. Since the link is supposed to be Rayleigh, the channel gain $|h|^2$ follows an exponential distribution of parameter μ (square of a Rayleigh r.v.). Assuming that the UE is affected by some interference due to other neighbouring BSs, one can define a signal-to-interference ratio : $\text{SIR} = P_r/I_{agg}$ where the aggregate interference is defined as $I_{agg} = \sum_i P_{ti}|h|_i^2 r_i^{-\alpha}$. In this case, the coverage probability $P(\theta)$ can be expressed as :

$$\begin{aligned} P(\theta) &= \mathbb{P}_{|h|^2, I_{agg}}\Big[\text{SIR} \geq \theta\Big] \\ &= \mathbb{P}_{|h|^2, I_{agg}}\Big[\frac{P_t|h|^2 r^{-\alpha}}{I_{agg}} \geq \theta\Big] \\ &= \mathbb{P}_{|h|^2, I_{agg}}\Big[|h|^2 \geq \frac{\theta I_{agg}}{P_t r^{-\alpha}}\Big] \\ &= \mathbb{E}_{I_{agg}}\Big[\mathbb{P}_{|h|^2|I_{agg}}\Big[\frac{\theta I_{agg}}{P_t r^{-\alpha}}\Big]\Big] \\ &\overset{(1)}{=} \mathbb{E}_{I_{agg}}\Big[exp\Big(-\mu\frac{\theta I_{agg}}{P_t r^{-\alpha}}\Big)\Big] \\ &\overset{(2)}{=} \mathcal{L}_{I_{agg}}(s)\Big|_{s=\frac{\mu\theta}{P_t r^{-\alpha}}}, \end{aligned} \tag{2.5}$$

where (1) follows from the definition of the cdf of an exponential rv, and (2) from the definition of the LT. The main advantage of the Rayleigh fading assumption is that it quite straightforwardly leads to expressions relying on the LT of the interference. However, this model ignores the large scale nature of shadowing since it only accounts for the small scale fading using variable h. Besides, this rv is supposed to have the same distribution on every link, which makes little physical sense.

2.2.2 The $\kappa - \mu$ shadowed fading

Because of the lack of complexity of the Rayleigh fading, models involving other distributions have been developed.

The lognormal distribution has raised a lot of interest thanks to its physical interpretation. Large scale buildings in urban areas are one major source of shadowing. The loss per building can be expressed as βl. In this expression, l is the distance travelled by the wave through the medium, and β a loss per meter (expressed in dB). Since the signal between a BS and a UE is likely to cross a number N of buildings, the total loss will be of the form $\sum_{i=1}^{N} \beta_i l_i$. For large values of N, this expression will tends a Gaussian rv thanks to the Central limit theorem (CLT) [Misc63]. Expressed in linear scale, the resulting gain is thus lognormal.

The inverse Gaussian and Gamma distributions are also used to model large scale shadowing ([Sh11]). Furthermore, the Ricean and Nakagami distributions have been proven to be efficient to model multipath fading with strong LOS components (e.g. rural areas).

The emergence of 5G and heterogeneous networks requires however more global models that should be valid for a wide range of environments (indoors, outdoors, with small scale fading/shadowing, etc). The $\kappa - \mu$ distribution meets these requirements since it encompasses many of the models proposed so far in the literature ([Sh11]). It also fits very well to measurements made in practical scenarios. The probability distribution of a $\kappa - \mu$ random variable X is given by

$$f_X(x) = \frac{\theta_1^{m-\mu} x^{\mu-1}}{\theta_2^m \Gamma(\mu)} exp\Big(-\frac{x}{\theta_1}\Big)_1 F_1\Big(m;\mu;\frac{\theta_2-\theta_1}{\theta_1\theta_2}x\Big). \tag{2.6}$$

In this expression, $\theta_1 = \frac{\mathbb{E}[h]}{\mu(\kappa+1)}$ and $\theta_2 = \frac{(\mu\kappa+m)\mathbb{E}[h]}{\mu m(1+\kappa)}$ and ${}_1F_1(;;)$ is the confluent hypergeometric function. Since this function is not convenient, the pdf (and the LT) are often rewritten using Laguerre polynomial series expansions in order to have more tractable results.

The distribution has 3 parameters :

- m, that accounts for the presence of small scale shadowing.
- κ , that indicates the impact of a dominant component in the multipath links.
- μ, which is proportional to the number of scattering clusters.

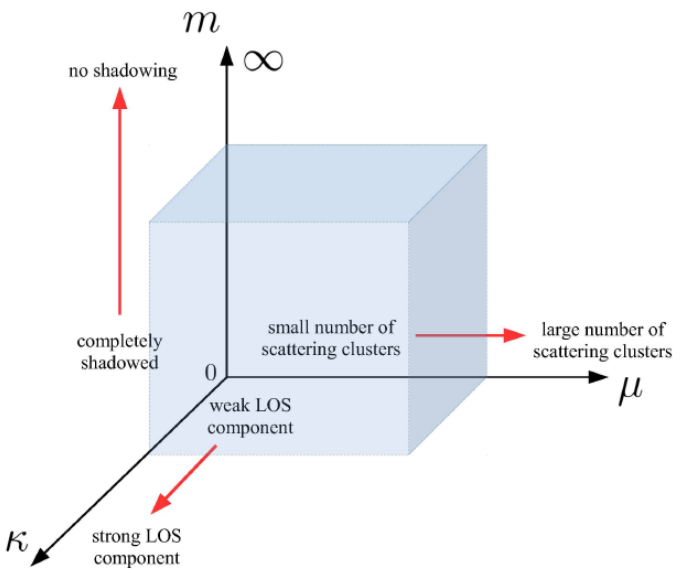

Figure 2.3: Physical interpretation of the parameters of the $\kappa - \mu$ distribution (Source : [Sh11])

For specific values of these parameters, we obtain as particular cases the distributions discussed before (see figure 2.4). Generalizations of this distribution have been conducted for MIMO scenarios by means of random matrix theory (see [Sh12]). Several authors prefer representing the fading and the shadowing using the distinct rv, in which case we use the term *composite channel model*. A current trend is to model channels using a $\kappa-\mu$ rv to account for fading and small scale shadowing, multiplied by another rv representing large scale shadowing [Sh11].

In summary this model is elegant in the sense that it covers a wide range of distributions. However it can not account for physical correlation between the links. Indeed, since the r.v.s are mutually independent, two adjacent links affected by the same scatterers or obstacles might have very different gains. The results of the following section will address this issue.

	κ-μ fading	η-μ fading	κ-μ shadowed fading
Rayleigh	$\kappa \to 0, \mu = 1$	$\eta = 1, \mu = 0.5$	$\kappa \to 0, \mu = 1$ or $m = 1, \mu = 1$
Nakagami-m	$\kappa \to 0, \mu = m$	$\eta = 1, \mu = m/2$ or $\eta \to 0, \mu = m$	$\kappa \to 0, \mu = m$ or $m \to m, \mu = m$
Nakagami-n (Rice)	$\mu = 1$		$\kappa = K, \mu = 1, m \to \infty$
Nakagami-q (Hoyt)		$\mu = 0.5$	$\kappa = (1-q^2)/2q^2, \mu = 1, m = 0.5$
One-sided Gaussian	$\kappa \to 0, \mu = 0.5$	$\eta \to 0, \mu = 0.5$ or $\eta \to \infty, \mu = 0.5$	$\kappa \to 0, \mu = 0.5$ or $m = 0.5, \mu = 0.5$
κ-μ fading	κ, μ		$\kappa \to \kappa, \mu \to \mu, m \to \infty$
η-μ fading		η, μ	$\kappa = (1-\eta)/2\eta, \mu \to 2\mu, m = \mu$
Rician shadowed			$\kappa = K, \mu = 1, m = m$

Figure 2.4: Distributions related to the $\kappa - \mu$ model (Source : [Sh11])

2.2.3 Manhattan models

Recent developments using Manhattan Poisson Line processes (MPLP) manage to integrate correlation bewteen links in a systematic way [Sh13-Sh15]. A MPLP is a point process that can be used to generate lines in $\mathbb{R}^n$ in order to create an irregular grid structure.

In [Sh13], the grid is two-dimensional and represents an urban area. The lines model streets and the spaces between them are assumed to be buildings. BSs are randomly distributed in the different streets, and the distribution of the SIR at a typical user is derived. The authors make the distinctions between the LOS and NLOS links. The latter is modeled by means of an absorption coefficient. For a given link, this coefficient is set to the power of the number of buildings obstructing the path. The LT of the joint NLOS interference at two distinct locations is derived as well. As seen in the next chapter, several improvements can be brought to this channel model.

An adaptation to an indoor two-dimensional scenario is considered in [Sh14]. In this case, the lines and spaces of the MPLP represent walls and rooms of a virtually infinite building. The mean interference is shown to be proportional to the density of transmitters, and inversely proportional to the square of the absorption coefficient. The correlation of the interference between different rooms is analyzed as well (see figure 2.5). The tail of the SIR distribution is shown to be heavy and upper bounded by the Weibull distribution. Interestingly, it is proven that this tail would be lighter in the case of independent shadowing.

Finally, a three-dimensional indoor extension has been developed in [Sh15]. The wording *Poisson building* is used to qualify the MPLP grid. The transmit BSs are distributed along the edges of the rooms, which constitutes a Cox point process. The model is shown to be asymptotically equivalent to [Sh14] when the absorption coefficient of the horizontal surfaces (floors and ceilings) tends to zero.

The main shortcoming of these models is that they are exclusively applicable in very specific environments (characterized by a MPLP). The random shape theory, addressed in the next paragraph, is able to account for sparser distributions of obstacles.

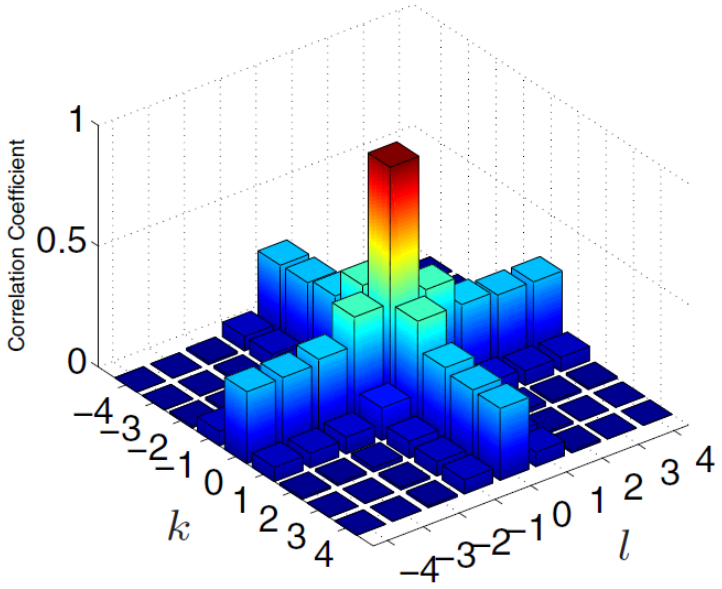

Figure 2.5: Correlation coefficient of the aggregate interference between the central room located in $(0, 0)$ and the other rooms located in (k, l) (Source : [Sh14])

2.2.4 Random shape theory

As mentioned here above, random shape theory is a branch of SG studying distributions of finite objects in $\mathbb{R}^n$. In [Sh16], the authors use a Boolean model to represent random obstacles as lines segments with random lengths and orientations. The distribution of the number of blockages over a path of given length is derived. An expression for the coverage probability for a Poisson network is obtained as function of the parameters of the blockages. Similar approaches are followed in [Sh18] and [Sh19] for rectangular and circular obstacles respectively.

The developments in [Sh17] go a step further in the sense that they integrate a form of macrodiversity : the UEs are able to connect to several BSs. The reliability probability is computed. This metric represents the probability for one UE to have at least one of its associated BS not being obstructed. Moreover, it is shown that increasing the average obstacle length increases the correlation between blockage events, which in turns results in a smaller diversity gain. The scenario of self-blocking (i.e. having a UE obstructed by its user) is analyzed as well. In that case the diversity gain is recomputed by modeling the body of the user as a cone. The presented results are, however, preliminary in the sense that they are not incorporated within an entire network model.

2.3 MIMO networks

2.3.1 Beamforming techniques

A major aspect of MIMO networks is the large number of degrees of freedom due to the presence of multiple antennas. Employing an optimal beamforming to exploit these degrees will also play an important role towards the development of 5G. Several beamforming techniques have been studied in [MIMO29-MIMO34].

The work in [MIMO30] compares the performances of the maximum ratio transmission (MRT) and the zero forcing (ZF) beamformings. Given a channel matrix $\mathbf{H}$, the corresponding precoding matrices are given by $\mathbf{W}^{ZF} = \mathbf{H}^{-1}$ and $\mathbf{W}^{MRT} = \mathbf{H}^{*}$. The analytical and numerical results

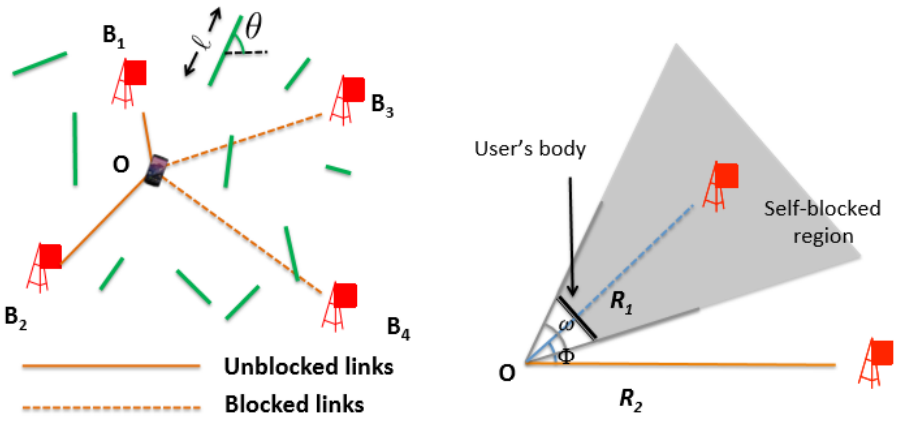

Figure 2.6: Left : Scheme of the model used in [Sh17]. Right : Self blocking model (Source : [Sh17])

tend to show that the latter yields better results in terms of capacity. However, the analysis is restricted to one cell. As a result, the model does not integrate extra cell interference. The developments in Chapter 4 will extend this model by modeling several BSs by means of a PP.

The approach followed in [MIMO29] considers UEs with multiple antennas. ZF beamforming is employed at both transmitter and receiver sides to minimize the intra and extra-cell interference respectively. The remaining antennas are used to improve the throughput and the useful power. An analytical expression of the spectral efficiency is derived using moment generating functions.

An uplink analysis is performed in [MIMO34]. It is shown that in an interference limited regime, a (super)linear scaling between the number of BSs and the number of UEs is necessary to maintain a certain SIR level. Fractional power control is applied as well.

2.3.2 Cooperative networks

Owing to bad channel conditions, it is often useful for a UE to achieve a diversity by connecting to more than one BS. In this case, the BSs must be coordinated and must exchange their respective channel state information (CSI). The higher the number of antennas, the larger the number of channels to estimate. A tradeoff is thus necessary between the cluster size (number of BSs sharing information) and the increase of overhead. This section covers several coordination techniques proposed in the literature [MIMO24-MIMO28] .

The framework in [MIMO24] enables receivers to connect to one or two adjacent BSs. The choice of BS association is performed by using the concept of second order Voronoi cells (figure 2.7). In the considered scenario, it is assumed that the BS only knows the phase information. An optimal association policy is derived. The UE connects to its two BSs when the ratio of the channel gains of its closest and second closest BS falls below a certain threshold. This threshold is computed to maximize the SIR level of the UE equipment. When a UE connects to two BSs, its information is splitted using Willem's encoding (with a common and a private part). It is shown that the global coverage increases by 17 % on average (compared to the same model with no coordination). The developments of this paper only involves one-antenna BSs.

The work in [MIMO25] generalizes the model of the previous paragraph in two directions. Firstly, the BSs are equipped with several transmit antennas. In addition, clusters including an

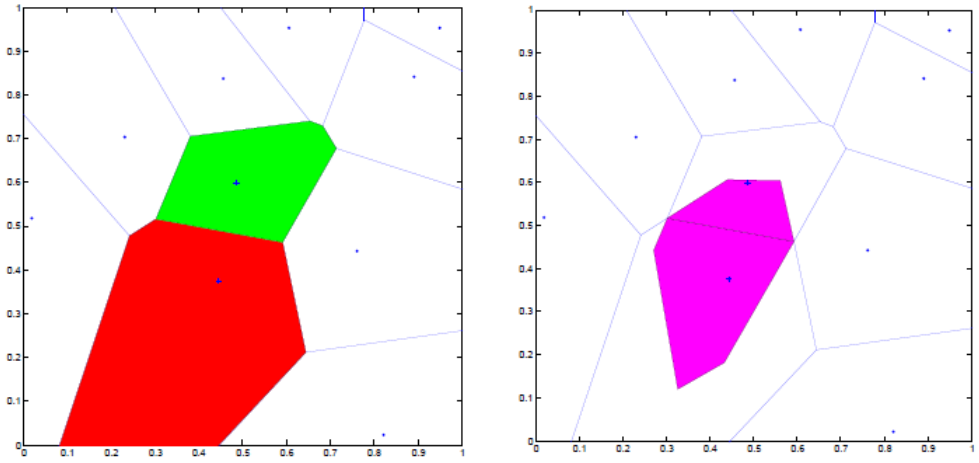

Figure 2.7: Left : 1-Voronoi tessellation - Right : 2-Voronoi tessellation (Source : [MIMO24])

arbitrary number of BSs are considered. The beamforming within each cluster is coordinated in order to maximize the received useful powers while nullifying the intracluster interference. Bounds for the coverage probability are computed as function of the cluster size and number of antennas per BS. The optimal cluster size is obtained by numerically optimizing the spectral efficiency (overheads included).

Cooperation in heterogeneous networks is studied in [MIMO26]. Two coordination techniques are compared. The first one consists in connecting the UE to the n BSs (among all the tiers) providing the strongest average power. The selected BS adjust their respective signals to transmit useful information to the user (without interference). The second strategy is similar, except that the UE mandatory connects to the closest BS of each tiers. The results suggest that the first technique is more efficient in terms of coverage.

2.3.3 Three-dimensional models

All the references cited above assume two dimensional transmission models. In the case of massive MIMO systems, the antennas are not necessarily placed on the same plane. Indeed, the array configuration can be rectangular, cylindrical, spherical, etc [MIMO22]. As a result, several effects must be considered for these 3D scenarios :

- First of all, the antenna pattern according to different elevation angles (*tilts*). This new degree of freedom should be taken into account to optimize the network performance ;
- Furthermore, the classical plane wave hypothesis is no longer verified. Spherical waves models are more accurate but come at the cost of higher complexity ;
- Since the arrays are very large, two antennas of the same array might not see the same scatterers. Antennas of a same BS are affected by different channel gains. The wording non-stationary channel is employed ;

In [MIMO22], the authors use an equivalent scatterer representation by means of a cylindrical model. Algorithms to design this representation are detailed. To define the channel of each antenna, it is assumed that the signal emitted by a given antenna is only affected by the scatterers present in a certain radius around this antenna (visibility sphere). The cross- and autocorrelation functions of the channel gain are derived as well.

The work in [MIMO23] covers directional antennas whose vertical tilt can be dynamically adjusted. The beamforming can therefore be adapted horizontally as well as vertically to minimize the intercell interference. A joint coordination strategy is established.

Although the models of the next chapters are two-dimensional, the 3D issues of massive MIMO systems should be considered for more practical simulation setups.

2.4 Power control algorithms

For the sake of tractability, most stochastic geometry-based models consider a constant transmit power for all BSs. Nevertheless, this assumption does not enable to exploit the potential degree of freedom in the power allocation. Indeed, tuning the values of the allocated powers can significantly improve the performance of the network. Various examples of power control algorithms are presented in [PC36]- [PC47].

The authors of [PC36] consider an adaptive algorithm to compute beamforming and the transmit powers in a joint manner. Such a problem generally requires to estimate every interfering link, which is typically performed by means of stochastic gradient methods. The main drawback of these methods is their implementation that can be rather challenging. The algorithm proposed in the paper overcomes this problem by means of projections on specific subspaces of the beamforming coefficients. A stochastic model is derived as well to evaluate the performance of the algorithm.

Many algorithms available in the literature are developed in the framework of cognitive networks. As a reminder, these networks consist in primary users (PUs, served by traditional multi-antenna BSs) as well as cognitive users (CUs, often assumed to be served by one-antenna BSs). Both are supposed to use the same time and frequency resources. In this scenario, the PUs have priority over CUs and must systematically have a sufficient quality of service (QoS). By contrast, the CUs attempt to transmit or receive information in an opportunistic manner. The values of their transmit power is thus crucial since they need to maximize their respective QoS whilst causing a limited amount of interference to the PUs. Power allocation in these cognitive networks is addressed in [PC37]- [PC39] for different objective functions. In [PC37], the CUs adapt their respective power thresholds according to a noncooperative game. It is proven that this game reaches a Nash equilibrium. The developments in [PC38] aim at optimizing the global network energy efficiency while taking into account a notion of fairness between the CUs. An alternating iterative scheme is proposed to this end. The work in [PC39] introduces the notion of pricing in the network model. There are now interactions between the PUs and CUs. The formers can now price the latter to control their interference and keep it under a certain threshold. Hence, the PUs can choose a price to maximize their revenues. Once this price is set, the CUs adjust their powers in turn to optimize their own revenues as well. These strategies are modeled by means of a Stackelberg game. Cognitive networks are not analyzed in this thesis and are thus left for potential future work. It is however worth mentioning them since they constitute a significant part of the literature on power control algorithms. Besides, some of the elements and techniques presented for cognitive networks are also applicable to traditional networks.

The results of [PC40] are particularly interesting since they are dedicated to heterogeneous networks. In particular, a power control algorithm is designed for the BSs belonging to femtocells of a two-tier network. Firstly, the aggregate interference of the network is shown to follow an alpha stable distribution. Then the emission amplitude B, supposed constant for all femtocell BSs, is adjusted to solve an optimization problem consisting in maximizing the QoS of femtocell users. The solution to this problem has to fulfill the following constraint : the interference coming from femtocell BSs and experienced by the macrocell users must statistically be below a certain

threshold. In other words, the ccdf of the interference $||Y_f||$ evaluated for the threshold value I_S should be below the value σ. The steps of the algorithms to solve this optimization problem are summarized in figure 2.8. First, the parameters of the alpha stable distribution α and γ are estimated thanks to the path loss exponent of the environment m and the density of femtocell access points λ_f. The emission amplitude is then iteratively adjusted in order to satisfy the interference constraint.

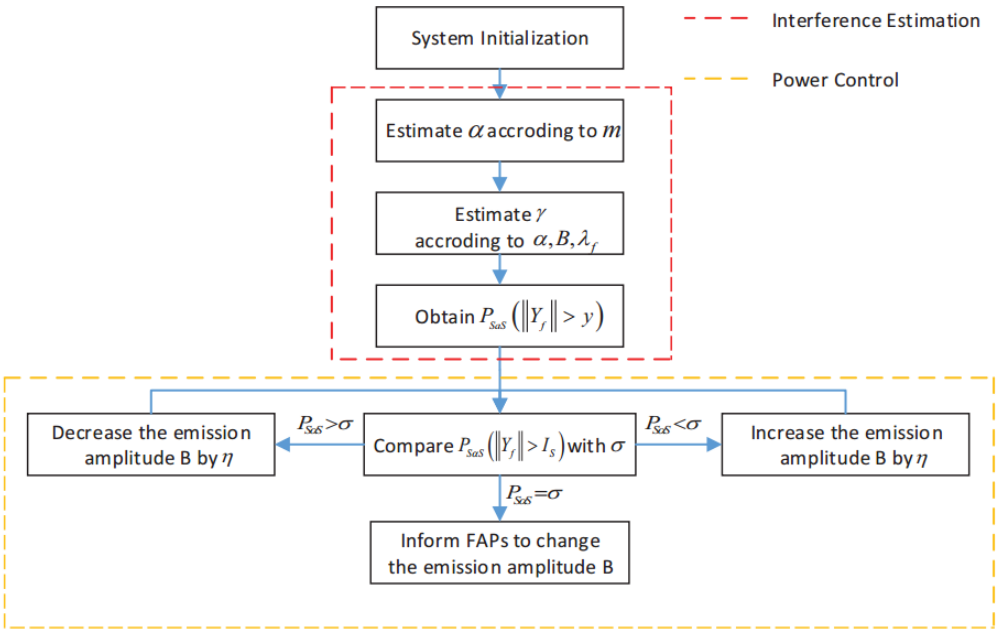

Figure 2.8: Flow diagram of the algorithm of [PC40] (source : [PC40])

Finally, the content of [PC41] proposes a general overview of power control schemes, including distributed power control, joint power control and BS assignment,etc. The algorithms presented in Chapter 5 are partly adapted from this source.

2.5 Heterogeneous networks

Hetnets are studied in [HetNet48-HetNet52] and [MIMO29]. Both [HetNet48] and [MIMO29] propose an analysis of a general K-tier MIMO network where the BSs are distributed by means of PPPs. In [HetNet48], LOS and NLOS links are modeled by means of m-Nakagami fading. The beamforming is supposed to be directional and is incorporated into the model using probabilistic effective antenna gains. By constrast, the work in [MIMO29] models beamformers in a more classical manner using precoding matrices. The coverage probability and the sprectral efficiency are analytically derived.

The authors of [HetNet49] analyze a two-tier network whose microcells are modeled using a Matern Cluster Process. An accurate expression for PGFL of this PP is derived, as well as a distribution function for the desired distance (distance between a UE and its serving microcell BS). These two formulations enable to obtain a tractable expression for the network coverage.

In [HetNet50], two frameworks are developed to analyze general Hetnets (whose nodes can be distributed using any PP). Both proposed methods are extensions of the ASAPPP approximation (Approximate SIR Analysis based on the PPP). The analysis relies on the observation that

general coverage curves of Hetnets are all approximately the same, up to a horizontal shift (expressd in dB). The method therefore consists in estimating the gain of the network with respect to its equivalent network generated using PPPs.

Finally the works of [HetNet51-HetNet52] are dedicated to resource allocation strategies. [HetNet51] proposes a stochastic-geometry based method to achieve an optimal load balancing in a two-tier network. The content of [HetNet52] is sligthly more specific : digital and hybrid (analog and digital) schemes are designed to transmit scalable information (e.g. video coding) over HetNets. A distorsion analysis is also performed for different spectrum allocation policies.

Chapter 3

Coverage estimation of a realistic urban shadowing model

Urban areas are typical environments where a relevant network deployment is crucial. City centers are usually characterized by a very high density of UEs to be served. With this aim in view, urban networks rely on large number of BSs that can be used within cells of variable size (HetNets). Because of the numerous BSs present around a typical user, the interference signals observed by the UE are likely to be significant and should be modeled with accuracy. These signals are impacted by shadowing and diffraction due to the buildings. An accurate analysis of these propagation mechanisms is therefore necessary.

The main contribution of this chapter consists in integrating a physically correlated shadowing model of the aggregate interference in a stochastic geometry-based approach. The considered shadowing takes place in a Manhattan urban grid and combines both penetration and corner diffraction when modeling signal transmission from base stations to users. Tractable expressions for the network coverage probability are derived. Our initial results suggest that the diffracted mechanisms are dominant compared to building penetration.

Our model can be viewed as an extension of the work done in [Sh13] and has been partly presented in [Misc56]. Part of the content presented in this chapter is thus based on these two sources.

3.1 System model

3.1.1 Node distribution

The urban environment is first generated in a random manner. We consider an infinite irregular grid generated by two one-dimensional homogeneous PPPs. Let Φ_x and Φ_y these PPPs and λ_x and λ_y their intensities. The points generated by Φ_x and Φ_y are respectively placed on the horizontal and vertical axis on the plane $\mathbb{R}^2$. From each point is drawn an infinite line perpendicular to its axis. The generated set of lines represent streets in our model, and the spaces between these lines correspond to rectangular buildings. As seen in the previous chapter, the joint use of these PPPs is said to form a *Manhattan Poisson Line Process* (MPLP) and can be generalized to higher dimensions if more PPPs are employed. Considering variable intensities enables to extend the model of [Sh13] in which λ_x and λ_y are unitary.

BSs are then placed randomly in each street according to a third PPP Φ of intensity λ. An example of resulting grid is depicted in figure 4.1.

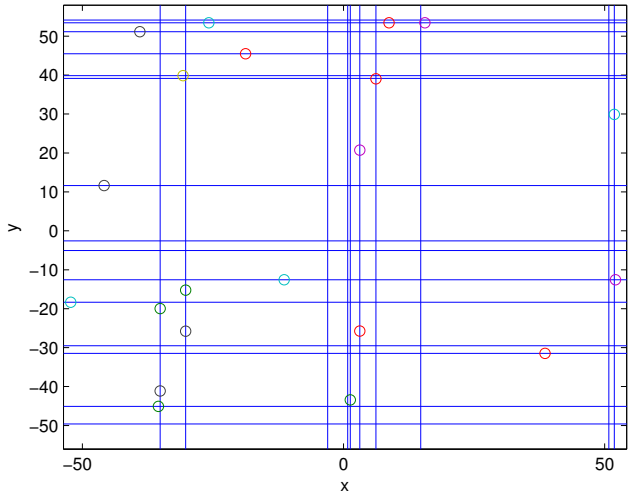

Figure 3.1: Example of Mahattan grid for $\lambda_x = \lambda_y = 0.1$ and $\lambda = 0.025$. The dots represent the BSs.

Since an infinite environment is assumed, the coverage should be invariant to the user location [Sh13]. The analysis of the next sections is thus performed for a typical user equipment. The coordinates of this UE are here given by $(0, y^*)$ where y^* is the ordinate of the horizontal street which is the closest to the x-axis. In practical simulation setups, it is however impossible to model such an infinite grid. Nevertheless, if one selects a sufficiently large size grid, the results converge to the infinite case.

3.1.2 Radio propagation model

Among all transmissions within the network, we will distinguish three types of received powers at the UE.

1. The line-of-sight (LOS) power coming from a base station x located in the same street as the UE y. Its expression is given by :

$$P_{xy}^{LOS} = P_{tx}|h_{xy}|^2 l_{out}(||x - y||). \tag{3.1}$$

   In this expression, P_{tx} is the transmit power and is here assumed to be unitary for all BSs; $|h_{xy}|^2 \sim Exp(1)$ is a random variable accounting for fading effects on the link. Finally, the distance is taken into account using the standard path loss function:

$$l_{out}(z) = Bz^{-\alpha_{out}}. \tag{3.2}$$

   We consider here a constant unitary amplitude $B = 1$ and a path loss exponent α_{out} of 3, typical for outdoor urban environments [Sh20].

2. The non-line-of-sight (NLOS) signals crossing buildings in a straight line to reach the UE. In [Sh13], it is assumed that the loss per building is constant. In this case, the expression of the received power is given by eq. (3.3) :

$$P_{xy}^{NLOS,obstr} = P_{tx}h_{xy}K^N, \tag{3.3}$$

where K is a constant absorption coefficient. This assumption is however reductive since the signals do not cross the same portions of the buildings in practice. For this reason, we propose a more realistic penetration model in eq. (3.4):

$$P_{xy}^{NLOS,obstr} = P_{tx}|h_{xy}|^2 l_{in}(||x-y||)g_e(N)g_i(||x-y||). \tag{3.4}$$

In this equation, the pass loss function l_{in} is redefined compared to the previous case because it uses a smaller path loss exponent α_{in} (we use a value of 1.7, which is typical for indoor environments [Sh20]). The function $g_e(N)$ represents the losses due to the external walls of the buildings and is defined as :

$$g_e(N) = 10^{w_e N/10}, \tag{3.5}$$

where N is the number of crossed buildings and $w_e = -14\ dB$ is the average loss per pair of walls with non-metallized windows [Misc64]. A second function g_i is used to model the losses caused by walls and obstacles inside the buildings.

$$g_i(||x-y||) = 10^{||x-y||w_i/10}. \tag{3.6}$$

Its parameter w_i represents the average loss per meter and is tuned to yield a total loss of -14 dB for an average size building. These parameters are illustrated in figure 3.2.

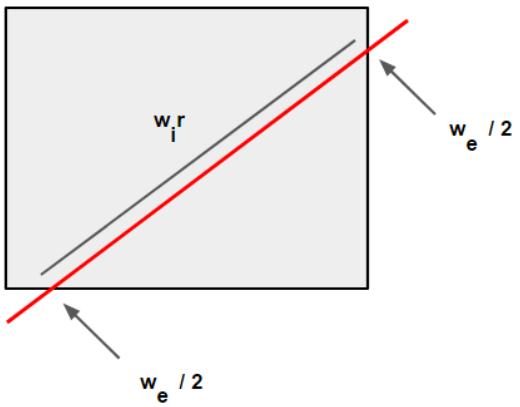

Figure 3.2: Illustration of the parameters w_e and w_i.

3. The NLOS signals diffracted around building corners are modeled thanks to Berg recursive model [Sh21].

   This framework assumes that each corner of street is acting as an independent source. The received powers are thus considered to be LOS. Therefore, equation 3.1 is again used as in the first case, but with a virtual distance d_j higher than the actual distance $||x-y||$. This distance d_j (where j is an index indicating the number of times the signal has encountered a corner) is defined recursively :

$$d_j = k_j s_{j-1} + d_{j-1}, \tag{3.7}$$

$$\text{with } k_j = k_{j-1} + d_{j-1}q_{j-1} \text{ and } q_j = q_{90}(\tfrac{\theta_j}{90^\circ})^\nu.$$

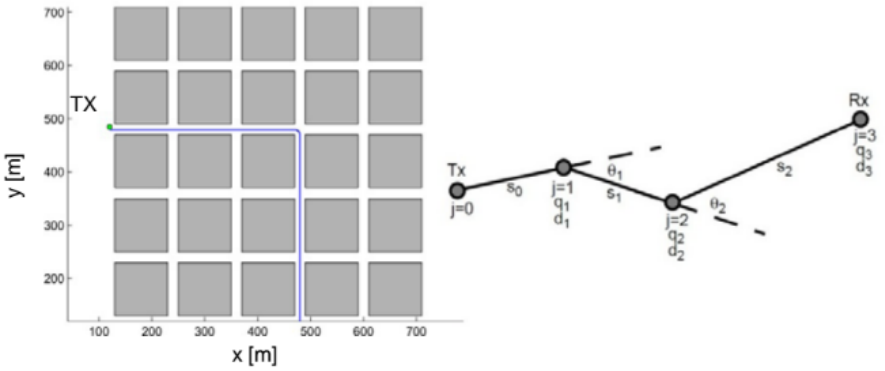

Figure 3.3: Berg recursive model (Source : [Sh20]).

As illustrated in figure 3.3, the variables d_j and s_j are respectively the actual and virtual distances. θ_i is the angle of every corner j. The other variables ν and q_{90} depend on the environment and are determined by means of empirical measurements. Since every corner of the grid forms a right angle, the value of ν do not have to be selected in our case. We here assume a constant value of 0.5 for q_{90}, since it is a usual value according to the fitting results in [Sh20]. For the sake of simplicity, we will here restrict the analysis to the first order model (i.e. neglecting the signals diffracted more than once).

In addition to the interference, the typical user is assumed to be affected by a constant background noise power W.

3.2 Coverage probability analysis

In this section, several analytical formulations are obtained to evaluate the coverage probability as performance metric of the network. Before going into details, let us say a few words about the contributions of this section with respect to the work in [Sh13]:

- proposition 2 was already available in [Sh13];
- proposition 3 and 4 were already available in [Sh13] but without their proofs which we provide here;
- proposition 1, 5, 6 and 7 are new with respect to the content of [Sh13].

The proofs of these results can be skipped without loss of information to read the other sections. They have however been intentionally left in the body of this document because they are interesting in terms of mathematics and hypotheses.

Let us recall that the coverage probability $P(\theta)$ is by definition the probability for the SINR to be greater than a threshold variable θ. In other words, $P(\theta) = \mathbb{P}(\text{SINR} > \theta)$. This probability can be characterized according to the association policy.

Proposition 1 : Under closest LOS BS association, the coverage probability of a typical user is given by :

$$P_{C-LOS}(\theta) = 2\lambda \int_0^\infty \mathcal{L}_W(s)\Big|_{s=\frac{\theta}{P_t l_{out}(x)}} \mathcal{L}_{I_{LOS}}(s)\Big|_{s=\frac{\theta}{P_t l_{out}(x)}} \mathcal{L}_{I_{NLOS}}(s)\Big|_{s=\frac{\theta}{P_t l_{out}(x)}} exp(-2\lambda x)dx. \tag{3.8}$$

Proof : The coverage probability can be expressed by means of the following equalities :

$$\begin{aligned}
P(\theta) &= \mathbb{P}_{|h|^2, I_{agg}, W}\Big[SIR \geq \theta\Big] \\
&= \mathbb{P}_{|h|^2, I_{agg}, W}\Big[\frac{P_t|h|^2 l_{out}(x)}{I_{agg}+W} \geq \theta\Big] \\
&= \mathbb{P}_{|h|^2, I_{agg}, W}\Big[|h|^2 \geq \frac{\theta(I_{agg}+W)}{P_t l_{out}(x)}\Big] \\
&= \mathbb{E}_{I_{agg}}\Big[\mathbb{P}_{|h|^2|I_{agg}}\Big[\frac{\theta(I_{agg}+W)}{P_t l_{out}(x)}\Big]\Big] \\
&\overset{(1)}{=} \mathbb{E}_{I_{agg}}\Big[exp\Big(-\frac{\theta(I_{agg}+W)}{P_t l_{out}(x)}\Big)\Big] \\
&\overset{(2)}{=} \mathbb{E}_{I_{agg}}\Big[exp\Big(-\frac{\theta I_{agg}}{P_t l_{out}(x)}\Big)\Big]\mathbb{E}_W\Big[exp\Big(-\frac{\theta W}{P_t l_{out}(x)}\Big)\Big] \\
&\overset{(3)}{=} \mathcal{L}_{I_{agg}}(s)\Big|_{s=\frac{\theta}{P_t l_{out}(x)}} \mathcal{L}_W(s)\Big|_{s=\frac{\theta}{P_t l_{out}(x)}} \\
&\overset{(4)}{=} \mathcal{L}_{I_{LOS}}(s)\Big|_{s=\frac{\theta}{P_t l_{out}(x)}} \mathcal{L}_{I_{NLOS}}(s)\Big|_{s=\frac{\theta}{P_t l_{out}(x)}} \mathcal{L}_W(s)\Big|_{s=\frac{\theta}{P_t l_{out}(x)}}.
\end{aligned} \tag{3.9}$$

In this proof, equality (1) is obtained using the ccdf of the exponential rv $|h|^2$, (2) comes from the independence of the noise and the interference, (3) is obtained using the definition of the LT and (4) is the result of the independence between the LOS and NLOS interferences. As a last step, it is necessary to average eq. (3.9) over the distance x to the closest BS. The pdf of this distance can be expressed as derivative of the complementary function of the void probability of a PPP [SG5]. Its expression is given in eq. (3.10) :

$$f_X(x) = 2\lambda exp(-2\lambda x). \tag{3.10}$$

Proposition 2 : Under strongest LOS BS association, the coverage probability of a typical user is given by (3.11).

$$P_{S-LOS}(\theta) = 2\lambda \int_0^\infty \mathcal{L}_W(s)\Big|_{s=\frac{\theta}{P_t l_{out}(x)}} \mathcal{L}^2_{ILOS}(s)\Big|_{s=\frac{\theta}{P_t l_{out}(x)}} \mathcal{L}_{I_{NLOS}}(s)\Big|_{s=\frac{\theta}{P_t l_{out}(x)}} dx. \tag{3.11}$$

The proof of this theorem is based on Campbell theorem [SG5].

Propositions 3 to 7 give expressions for the Laplace transforms needed in propositions 1 and 2 according to the different propagation models of the previous section.

Proposition 3 : The LT of the noise power can be expressed as:

$$\mathcal{L}_W(s) = exp(-Ws). \tag{3.12}$$

The proof is trivial since W is here assumed to be constant. It is hence sufficient to apply the definition of the LT.

Proposition 4 : The LT of the LOS interference is given by :

$$\mathcal{L}_{I_{LOS}}(s) = exp\Big(- \lambda \int_0^\infty \frac{sl_{out}(x)}{1 + sl_{out}(x)} dx\Big). \tag{3.13}$$

Proof : Let Ψ_{LOS}, the set of BSs in the same street as the typical user and let x_i and $|h_i|^2$ the distance and channel gain between a BS $i \in \Psi_{LOS}$ and the typical user. The LT of the total LOS interference can be expressed as :

$$\begin{aligned}
\mathcal{L}_{I_{LOS}}(s) &= \mathbb{E}_{|h_i|^2, x_i}\Big[exp\Big(- s \sum_{i \in \Psi_{LOS} \setminus i^*} |h_i|^2 x_i^{-\alpha}\Big)\Big] \\
&\overset{(1)}{=} \mathbb{E}_{|h_i|^2, x_i}\Big[exp\Big(- s \sum_{i \in \Psi_{LOS}} |h_i|^2 x_i^{-\alpha}\Big)\Big] \\
&= \mathbb{E}_{x_i}\Big[\prod_{i \in \Psi_{LOS}} \mathbb{E}_{h_i}\big[exp(- s|h_i|^2 x_i^{-\alpha})\big]\Big] \\
&\overset{(2)}{=} \mathbb{E}_{x_i}\Big[\prod_{i \in \Psi_{LOS}} \frac{1}{1 + sl_{out}(x_i)}\Big] \\
&\overset{(3)}{=} exp\Big(- \lambda \int_0^\infty 1 - \frac{1}{1 + sl_{out}(x)} dx\Big).
\end{aligned} \tag{3.14}$$

Slivnyak's theorem is used in equality (1) and states that properties of the PPP Ψ_{LOS} are unchanged when removing the BS i^* to which the user is connected. (2) relies on the LT of an exponential random variable. Eq. (2.2) expressing the PGFL of a PPP is used to prove (3).

Proposition 5 : The LT of the NLOS obstructed interference using the simplified expression 3.3 (with a constant loss factor) is given by :

$$\mathcal{L}_{NLOS}(s) = \left(\prod_{i>0} \frac{\lambda_x \lambda_y}{\Big[\lambda_x + 2\lambda \sum_{j>0} \frac{sK^{i+j-1}}{1+sK^{i+j-1}}\Big]\Big[\lambda_x + 2\lambda \sum_{j>0} \frac{sK^{i+j-1}}{1+sK^{i+j-1}}\Big]} \right)^2. \tag{3.15}$$

Proof : To prove this result, it is necessary to label the street segments of the grid as indicated in figure 3.4.

Let U_{ij} and V_{ij}, the number of BSs in street segments u_{ij} and v_{ij}. These numbers follow a Poisson law of parameters x_i and y_j representing the lengths of the horizontal and vertical segments respectively. The number of buildings crossed to reach the typical user (located at the origin in figure) from these streets is equal to $|i| + |j| - 1$. The total NLOS interference can hence be written in the following way :

$$I_{NLOS} = \sum_{i \in \mathbb{Z}} \sum_{j \in \mathbb{Z}} \left[P_t K^{|i|+|j|-1}\Big(\sum_{m=1}^{U_{ij}} |h_{ijm}|^2 + \sum_{n=1}^{V_{ij}} |h_{ijn}|^2\Big)\right], \tag{3.16}$$

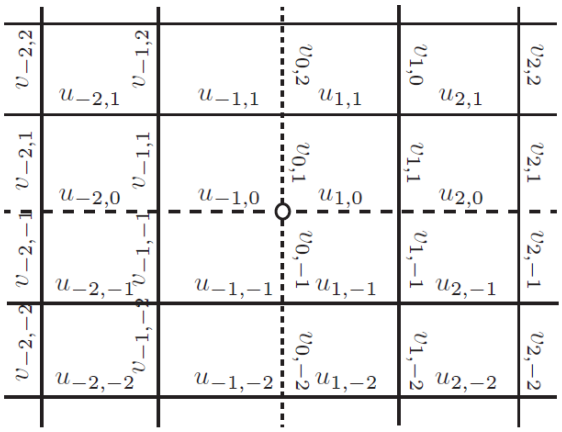

Figure 3.4: Source : Labeling convention of the grid [Sh13]

where $|h_{ijm}|^2$ represents the channel gain of the mth user located in horizontal segment ij. The LT of 3.16 conditioned to the MPLP can be expressed as:

$$\begin{aligned}
\mathcal{L}_{NLOS|\Psi_x,\Psi_y}(s) &= \mathbb{E}\left[e^{-sI_{NLOS}}\right] \\
&\overset{(1)}{=} \prod_{i\in\mathbb{Z}}\prod_{j\in\mathbb{Z}} \mathbb{E}_{U_{ij}}\left[e^{-sK^{|i|+|j|-1}\sum_{m=1}^{U_{ij}}|h_{ijm}|^2}\right].\mathbb{E}_{V_{ij}}\left[e^{-sK^{|i|+|j|-1}\sum_{m=1}^{V_{ij}}|h_{ijn}|^2}\right] \\
&\overset{(2)}{=} \prod_{i\in\mathbb{Z}}\prod_{j\in\mathbb{Z}} e^{\lambda x_i \frac{-sK^{|i|+|j|-1}}{1+sK^{|i|+|j|-1}}} e^{\lambda y_j \frac{-sK^{|i|+|j|-1}}{1+sK^{|i|+|j|-1}}} \\
&= \prod_{i\in\mathbb{Z}} e^{\lambda x_i \sum_{j\in\mathbb{Z}} \frac{-sK^{|i|+|j|-1}}{1+sK^{|i|+|j|-1}}} . \prod_{j\in\mathbb{Z}} e^{\lambda y_j \sum_{i\in\mathbb{Z}} \frac{-sK^{|i|+|j|-1}}{1+sK^{|i|+|j|-1}}}.
\end{aligned} \tag{3.17}$$

Equality (1) comes from the independence of the numbers of BSs in the different streets. (2) is based on the LT of a Poisson number (U_{ij} and V_{ij}) of exponential random variables ($|h_{ijm}|^2$ and $|h_{ijn}|^2$) [Sh13]. The expression obtained in eq. (3.17) needs to be averaged over all possible MPLP realisations. The random variables that remain in this expression are the distance x_i and y_j. These parameters can be viewed as lengths of interval separated two successive realizations of the same one-dimensional PPP. It is possible to show that they follow exponential distributions of respective parameters $1/\lambda_x$ and $1/\lambda_y$ [Misc57]. As a consequence, the unconditional NLOS LT can be expressed as :

$$\begin{aligned}
\mathcal{L}_{NLOS}(s) &= \prod_{i\in\mathbb{Z}} \mathbb{E}_{x_i}\left[e^{\lambda x_i \sum_{j\in\mathbb{Z}} \frac{-sK^{|i|+|j|-1}}{1+sK^{|i|+|j|-1}}}\right] . \prod_{j\in\mathbb{Z}} \mathbb{E}_{y_j}\left[e^{\lambda y_j \sum_{i\in\mathbb{Z}} \frac{-sK^{|i|+|j|-1}}{1+sK^{|i|+|j|-1}}}\right] \\
&\overset{(1)}{=} \prod_{i\in\mathbb{Z}} \frac{\lambda_x}{\lambda_x + \lambda \sum_{j\in\mathbb{Z}} \frac{sK^{|i|+|j|-1}}{1+sK^{|i|+|j|-1}}} \prod_{j\in\mathbb{Z}} \frac{\lambda_y}{\lambda_y + \lambda \sum_{i\in\mathbb{Z}} \frac{sK^{|i|+|j|-1}}{1+sK^{|i|+|j|-1}}} \\
&\overset{(2)}{=} \prod_{i>0} \left(\frac{\lambda_x}{\lambda_x + 2\lambda \sum_{j>0} \frac{sK^{|i|+|j|-1}}{1+sK^{|i|+|j|-1}}}\right)^2 \prod_{j>0} \left(\frac{\lambda_y}{\lambda_y + 2\lambda \sum_{i>0} \frac{sK^{|i|+|j|-1}}{1+sK^{|i|+|j|-1}}}\right)^2.
\end{aligned} \tag{3.18}$$

The LT of an exponential distribution is applied in equality (1). (2) uses the fact that the expression is even with respect to the values of indexes i and j since they are in absolute values.

Proposition 6 : The LT of the NLOS obstructed interference using the model of eq. (3.4) can be estimated by the following expression:

$$\mathcal{L}_{NLOS}(s) \sim \int_0^\infty \frac{1}{x\sqrt{2\pi}\sigma} exp(-sx - \frac{(log(x)-\mu)^2}{2\sigma^2}) dx, \tag{3.19}$$

where μ and σ can be estimated numerically.

Justification : eq. 3.4 is recalled below :

$$P_{xy}^{NLOS,obstr} = P_{tx}|h_{xy}|^2 l_{in}(||x-y||)10^{w_e N/10}10^{||x-y||w_i/10}.$$

Since this equation is more complex than eq. 3.3, it is not possible to use the same reasoning as in proposition 5. Indeed, the LT conditioned to the MPLP would be given by an expression similar to eq. (3.17), except that the terms $K^{|i|+|j|-1}$ would be replaced by the heavier factors given in eq. (3.4). These factors depend on the MPLP in a nonlinear manner. Besides, they have different distributions and are multiplying each other. As a result, taking their LT or their product would require to convolve their respective LTs, which is not analytically possible. One might think of approximating the distribution of the contribution of each BS (given by eq. (3.4)) by a known distribution. To the best of the author's knowledge, no such closed form distribution is available in the literature.

For this reason, we will try to analyze the total aggregate NLOS interference. After running Monte Carlo simulations, the pdf of this global interference has been numerically estimated. As shown in figure 3.5, the pdf tends to a normal distribution for values expressed in logarithmic scale. This means that the interference values expressed in linear scale follow a lognormal distribution. The LT of this distribution in hence given in integral form in eq. (3.19). Approximations of this integral are available in [Misc58].

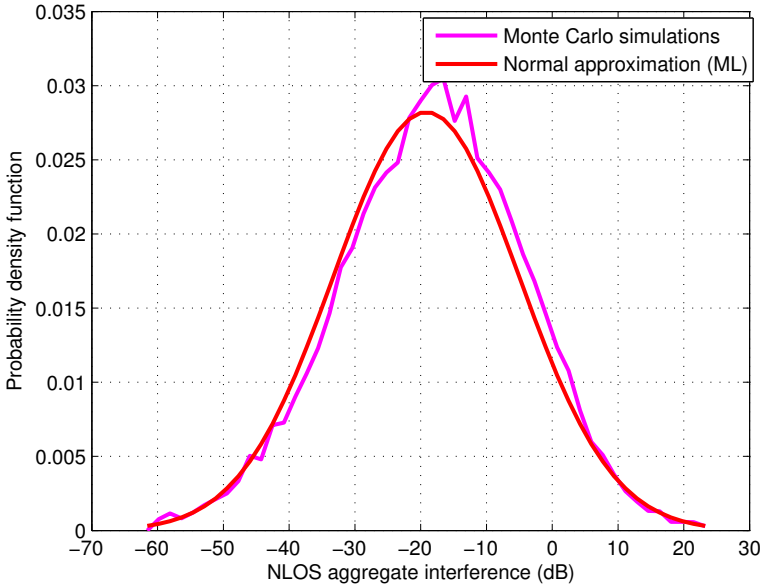

Figure 3.5: The purple curve represents the pdf of the aggregate NLOS interference (expressed in dB) for $\lambda = 0.1$ and $\lambda_x = \lambda_y = 1$. The red curve represents the pdf of a normal distribution whose parameters are estimated by applying the maximum likelihood method on the simulation results.

This result confirms the ideas presented in section 2.2.2 justifying the use of lognormal distribution to model shadowing. The drawback of this approach is that the values of μ and σ must be numerically evaluated and hence do not explicitly depend on the macroparameters.

Proposition 7 : The LT of the NLOS diffracted interference given in (3.7) can be estimated by the following expression:

$$\mathcal{L}_{NLOS,d}(s) \sim \left(\prod_{j>0} \frac{\lambda_y}{\lambda_y + 2\lambda \sum_{i>0} \frac{1}{1+\left(s(\frac{j-0.5}{\lambda_y} + \frac{i}{\lambda_x} + q_{90}\frac{(j-0.5)i}{\lambda_x \lambda_y}) \right)^{\alpha_{out}}}} \right)^2 . \tag{3.20}$$

Proof : this proof is based on two hypotheses :

- we assume that the BSs are all located in the middle of their respective street segments ;
- we assume that these segments have constant lengths, given by λ_x^{-1} and λ_y^{-1} for the horizontal and vertical streets.

Since we neglect signals diffracted more than once in Berg model, only the BSs located in the vertical streets cause significant interference to the typical user (located in a horizontal segment). The distances to be crossed (indicated in figure 3.6) can be expressed as the sums of the lengths of the traveled segments.

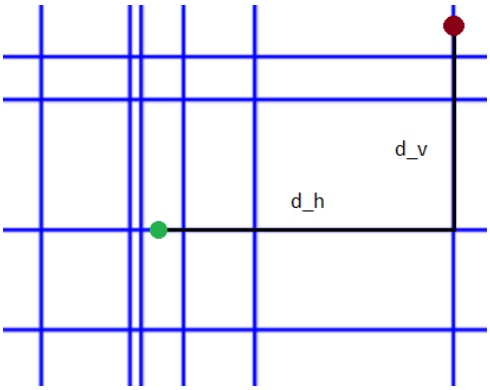

Figure 3.6: Representation of the distances in Berg model. The green point represents the typical user whilst the red point represents a BS.

Using eq. (3.7), the diffracted power received at the typical user coming from segment $v_{i,j}$ (containing $V_{i,j}$ BSs) is given by :

$$\begin{aligned} P_{ij} &= \sum_{n=1}^{V_{ij}} P_t |h_{ijn}|^2 (d_h + d_v + q_{90} d_v d_h)^{-\alpha_{out}} \\ &= \sum_{n=1}^{V_{ij}} P_t |h_{ijn}|^2 (\frac{|i|-0.5}{\lambda_x} + \frac{|j|-0.5}{\lambda_y} + q_{90}\frac{(|i|-0.5)(|j|-0.5)}{\lambda_x \lambda_y})^{-\alpha_{out}}. \end{aligned} \tag{3.21}$$

The aggregate diffracted interference can hence be expressed in the following way :

$$I_{NLOS,d} = \sum_{i\in\mathbb{Z}} \sum_{j\in\mathbb{Z}} \left[P_t \Big(\frac{|i|-0.5}{\lambda_x} + \frac{|j|-0.5}{\lambda_y} + q_{90}\frac{(|i|-0.5)(|j|-0.5)}{\lambda_x \lambda_y} \Big)^{-\alpha_{out}} \Big(\sum_{n=1}^{V_{ij}} |h_{ijn}|^2 \Big) \right]. \tag{3.22}$$

In a similar manner to the attenuation coefficient $K^{|i|+|j|-1}$ in eq. (3.16) the path loss term only depends on the indexes i an j. The rest of the proof therefore follows the same reasoning as the proof of proposition 5.

3.3 Numerical results

The following setup parameters have been used for all simulations : $\alpha_{out} = 3$, $\alpha_{in} = 1.7$, $w_e = -14dB$ and w_i tuned to obtain an average loss of -14dB/building.

3.3.1 Comparison of propagation mechanisms

Before simulating a large scale network, the validity of the signal models of section 3.1 has been tested by means of the following scenario : two BSs A and B are respectively placed on the upper left and lower right corners of a 3×3 regular grid. A user travels from A to B according to the red path displayed in figure 3.7.

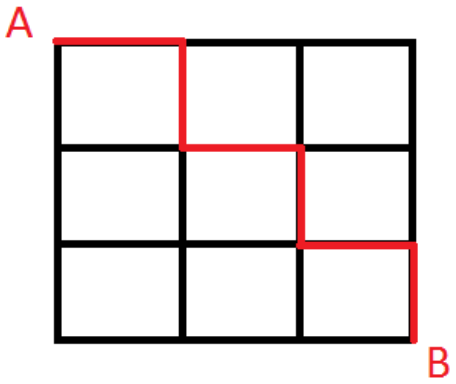

Figure 3.7: Trajectory of a user on a 3x3 regular grid.

The model of eq 3.4 is used to model the building penetration losses. We consider here a grid of size 50×50. The signals received by the UE are displayed in figure 3.8 as function of the distance travelled.

As shown on the graph, the curves for the diffracted and the obstructed signals do not evolve in the same manner. The power penetrating through the building is almost discontinuous. Indeed, as soon as the user turns around a corner, the signals have to cross one more building (and are therefore affected by the loss of -14 dB due to the external walls). Another important point is that the diffracted power from a given BS is almost always higher than the obstructed power from the same BS.

3.3.2 Monte Carlo simulations

Impact of the density of base stations

Figure 3.9 displays the coverage of the network for $\lambda_x = \lambda_y = 0.5$ and $\lambda = 0.3$ or 0.6. The diffracted paths and the noise are here neglected and the simplified model of eq. (3.3) is used to model the building attenuation (with $K = -10\ dB$). The typical user receives its useful power from the strongest LOS BS.

As depicted in the graph, the analytical curves (obtained by means of propositions 2,3 and 5) are coherent with the numerical curves. One can also deduce that increasing the density of

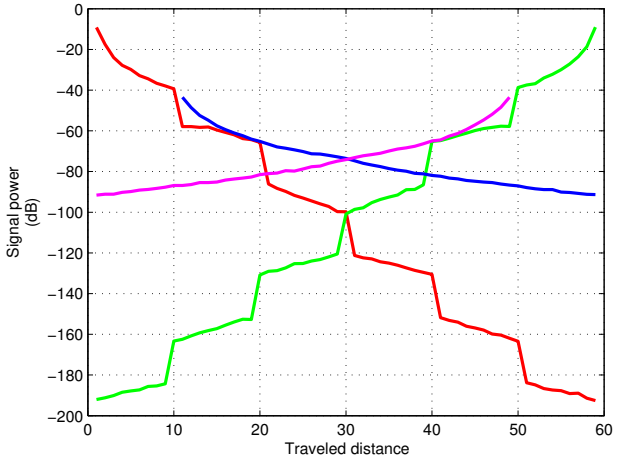

Figure 3.8: Signal levels as function of the position of the UE: red - LOS or NLOS (through buildings) power from BS A; blue - NLOS diffracted power from BS A; green - LOS or NLOS (through buildings) power from BS B; purple - NLOS diffracted power from BS B.

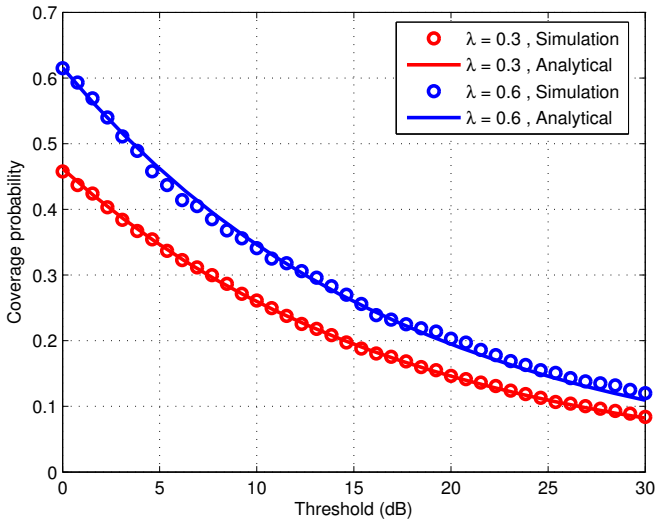

Figure 3.9: Comparison of the network coverages for $\lambda = 0.3$ and $\lambda = 0.6$.

BSs per street improves the global coverage. There are more interferers per street. However, the typical user can connect to a BS offering more power on average (since there are statistically more BSs in its own street as well).

Impact of the density of streets (without diffraction)

In figure 3.9, we consider the case of a varying densities of streets λ_x and λ_y for a constant $\lambda = 0.3$.

One can observe that the coverage increases with the densities of streets. This result, although counterintuitive, can be explained in the following way. First of all, the LOS interfering and useful powers do not depend on λ_x and λ_y (since they come from BSs located in the same street as the typical user). Therefore, these powers are not responsible for the changes in the SINR distribution. The changes in the coverage values are hence due to the NLOS interfering BSs

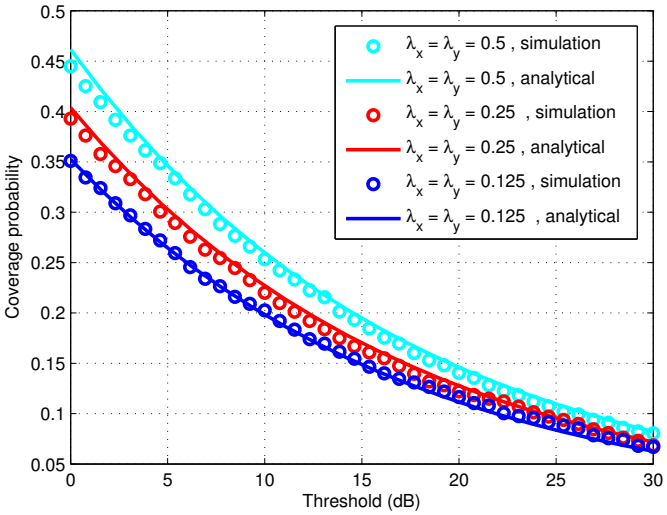

Figure 3.10: Comparaison of the network coverages for several values of the street densities (with K = -10 dB).

and can be illustrated it thanks to figure 3.11. Let us mention that both parts of the figure are displayed using the same scale and that the diffracted interference is not yet taken into account.

For an environment with a low density of streets (figure 3.11.a), the NLOS BSs are obstructed by a relatively small number of buildings. For example, the BSs in the street just under the street of the typical user (represented by red dots) are obstructed by at most 3 buildings. In particular, signals coming from BSs in the purple circle only need to cross one building to reach the user.

For an environment featuring a larger density of streets (figure 3.11.b), more BSs are present in the network. However, most of these BSs are separated by a larger number of buildings from the typical user. They do not contribute significantly to the total interference since they undergo more attenuation. Besides, one can see that the BSs in the street just under the street of the typical user are now obstructed by up to eight buildings (last red point on the right). Moreover, the zone of BSs in this street that are only blocked by one building (purple circle) is now much smaller. This means that the interfering BSs are obstructed by a larger number of buildings on average. For this reason, the total interference decreases.

Comparison of association policies

Figure 3.12 compares the strongest and closest BS association policies for $\lambda = 0.1$, $\lambda_x = \lambda_y = 0.5$ and $K = -10\ dB$. The analytical curves are thus obtained using either proposition 1 or proposition 2.

As expected, the graph suggests that the strongest BS association policy slightly improves the coverage. The simulation curve for the strongest BS association is not displayed on the graph for the sake of visibility but is coherent with the corresponding analytical purple curve.

Comparison of building attenuation models

The graph in figure 3.13 compares the coverage values obtained thanks to proposition 6 with simulations performed using the same set of density parameters : $\lambda = 0.1$, $\lambda_X = \lambda_y = 1$. We used here the strongest BS association policy. Since proposition 6 gives an approximation formula,

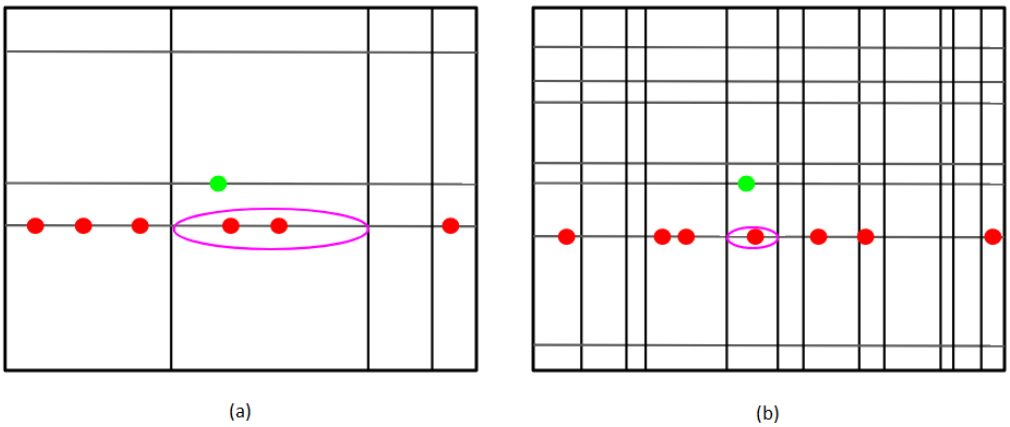

Figure 3.11: (a) - low street density, (b) high street density, in both cases the green point represents the typical user, the red points represent the BSs located in the horizontal street directly adjacent to the typical user, the purple zones contain BSs that are obstructed by one building only.

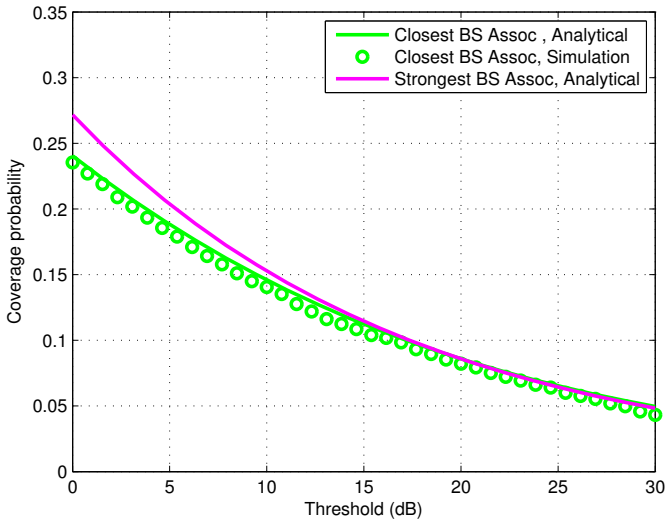

Figure 3.12: Comparison of the closest and strongest BS association policies.

the curves do not exactly superimpose each other. This is due to fact that μ and σ in eq. (3.19) are numerically estimated. Nevertheless, the estimation remains fairly accurate.

Figure 3.14 compares the model of eq. (3.4) (with variable penetration loss) with eq. (3.3) (with constant loss) for several values of the attenuation coefficient K. One can note that the simplified model produces values relatively close to 3.4 for $K \sim 38\ dB$. This observation makes sense in view of the parameters of 3.4. Indeed, the losses owing to external walls w_e are set to $-14\ dB$ per building and the losses caused the internal walls w_i are tuned to produce on average an attenuation of $-14\ dB$ as well. The rest of the attenuation is due to both indoor path loss and fading which represent 10 dB approximately.

A second comment can be made about figure 3.14. First, one can note that the coverage increases when the values of the coefficient K decrease. Indeed, the interference coming from NLOS BSs is more strongly attenuated. Interestingly, the coverage does not tend to one when

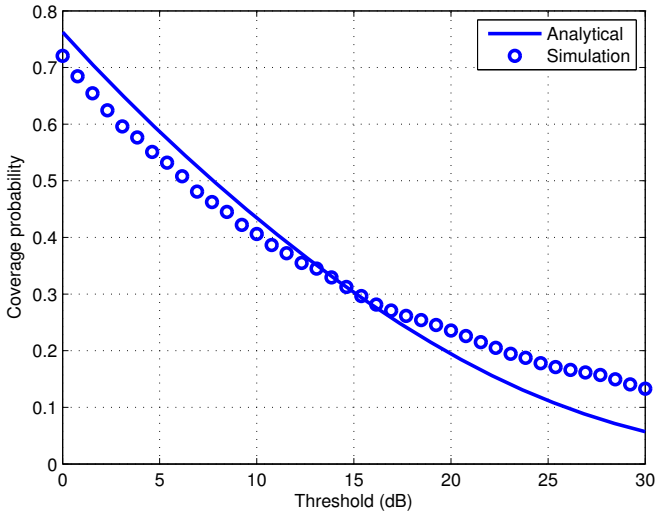

Figure 3.13: Comparison of Monte Carlo simulations with analytical values obatained by means of eq. (3.19) with $\mu = -19.45$ and $\sigma = 14.19$.

raising the values of K. The dotted curves of the graph are instead upper bounded by the discontinuous dark line corresponding to the case $K = -\infty$. This limit is due to the LOS interference coming from BSs located in the same street as the typical user. Actually, the dark line can also be obtained by computing the coverage ccdf of a one-dimensional network (corresponding her to the street of the typical user). A tractable expression for this network is available in [Sh13] and is given by $P(\theta) = sinc(\alpha^{-1})/\theta^{\frac{1}{\alpha}}$.

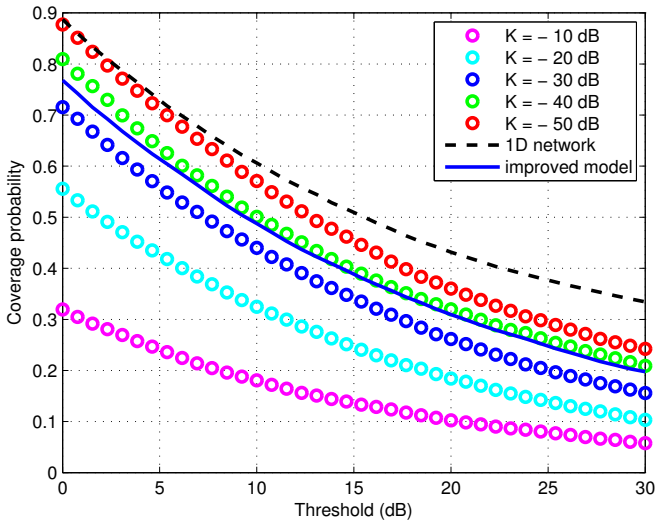

Figure 3.14: Comparison of the variable loss model (continuous blue curve) with constant loss model (dotted curves) plotted for several values of parameter K. The discontinuous dark curve represents the coverage of a one dimensional network.

Impact of the noise power

The validity of proposition 4 has been tested in figure 3.15. The chosen values of the noise power W are 10^{-4}, 10^{-3} and 10^{-2}, corresponding respectively to a mean a SNR of 21, 11 and 1 dB.

It is important to the note that the coverage values depicted in figure 3.15 are now related the SINR ratio.

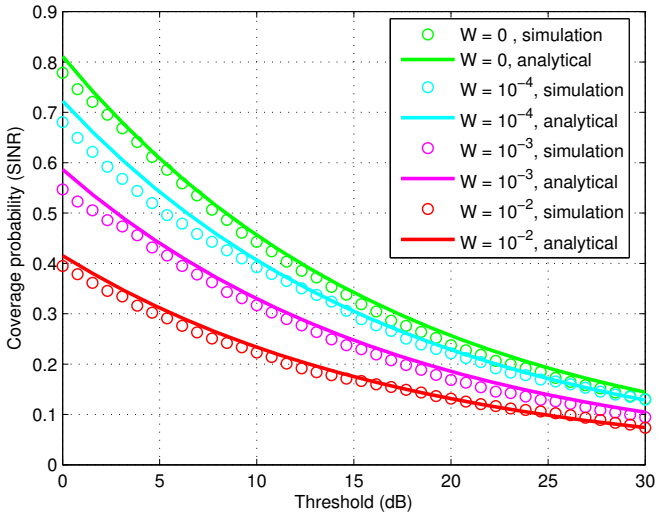

Figure 3.15: Impact of the noise power for $\lambda = 0.1$, $\lambda_x = \lambda_y = 1$ and $K = -38dB$.

Impact of the diffracted signals

We now introduce the diffracted signals in the simulations. Their impact is displayed in figure 3.16. The coverage significantly decreases when the diffraction mechanisms are taken into account (see red and blue dotted curves). This confirms the results of section 3.3.1 about the importance of the diffracted signals with respect to the obstructed signals. The analytical red curve has been obtained by means of proposition 7. Its values are sligthly above those obtained by simulation. This is due to the fact that proposition 7 assumes constant lengths of street segments. The case of very short segments in the neighbourhood of the typical user is hence not considered. The diffracted signals coming from this neighbourhood are much less attenuated and cause therefore a lot of interference. As a result, the analytical coverage values are slightly higher since this scenario is not covered.

Summary

Figure 3.17 displays the coverage (in terms of SINR) for the following choice of parameters and hypotheses :

- intensity parameters $\lambda = 0.1$, $\lambda_x = \lambda_y = 1$;
- variable penetration losses including using the model of eq. (3.4) ;
- diffracted signals included ;
- the noise power W set to 10^{-4} in order to produce a mean SNR of 21 dB, which is a realistic value in practical applications [Misc59].

One can note that the coverage values are too low to perform an efficient transmission. Indeed, the probability to have a SINR higher than 10 dB is of 18 %. This result in not surprising : the network is fully loaded in the sense that all users are served using the same resources. It would hence be relevant to separate them along a certain dimension to improve the SINR statistics. This will be performed in the next chapter in which beamforming techniques will be employed to make UEs orthogonal.

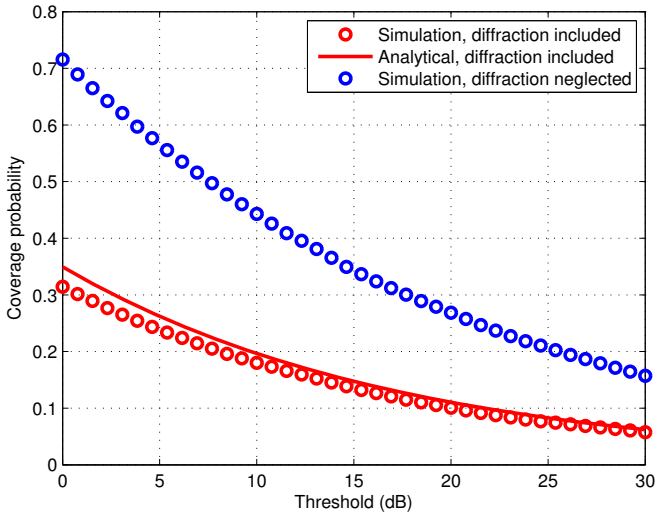

Figure 3.16: Impact of diffraction in the interference model. $\lambda = 0.1$, $\lambda_x = \lambda_y = 1$ and $K = -30\ dB$.

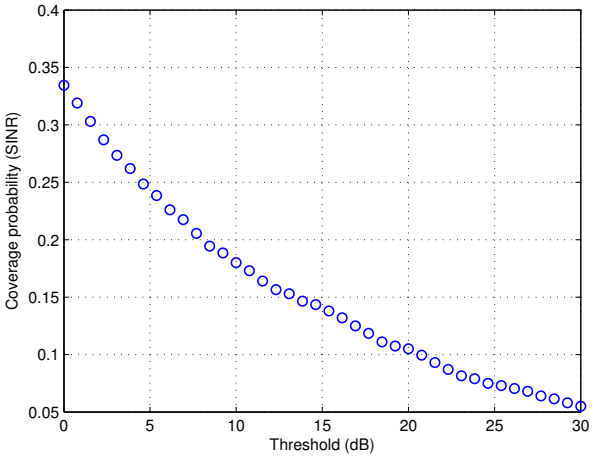

Figure 3.17: Impact of the noise power for $\lambda = 0.1$, $\lambda_x = \lambda_y = 1$ and $K = -38dB$.

Chapter 4

Coverage optimization strategies for massive MIMO networks

Since the development of the 3G technology, MIMO networks have played a key role to fulfill the constantly increasing needs of users in terms of data rate. Since this rate strongly depends on the SINR experienced by the UE, it is crucial to use all available resources to separate users and therefore to reduce the aggregate interference. These resources include time, frequency, code, and space. Whereas current available standards (3G and 4G) mainly use time and frequency division multiplexing, the upcoming 5G will rely more on MIMO systems and exploit space division multiplexing more intensively [Misc63].

Designing a massive multi-antenna network requires making several choices. It is first necessary to distribute the antennas on each BS and to position the BSs within the network. Moreover, a beamforming technique must be selected to reduce the interference between users served by the same BS. As mentioned in Chapter 2, the most studied methods for downlink transmissions are ZF and MRT beamforming. The orthogonality of UEs can be further improved if several adjacent BSs cooperate and exchange their CSI. In that case, the beamformers are computed by taking a larger number of interfering links into account. As a consequence, the interference of users served by adjacent BSs is minimized as well. In order to form these groups of neighbouring BSs, it is necessary to apply a clustering algorithm [MIMO25].

In this chapter, we consider a massive MIMO network constrained to a fixed global transmit power and a fixed total number of transmit antennas. Strategies are developed to optimize its downlink performance. Three possible degrees of freedom are analyzed : the distribution of the base stations, beamforming technique and the clustering method. Three different shadowing environments are considered as well. Our contribution consists in deriving analytical formulations to estimate the coverage of such massive MIMO networks (section 4.2) accounting for propagation conditions and clustering techniques. These expressions can be viewed as an optimization tool to maximize the global performance. We also present interpretations enabling to gain insight into the link between the performance of the beamformers and the propagation environment (section 4.3). Finally, methods are provided in order to enhance the clustering of the BSs (section 4.4).

Part of the content of this chapter has been submitted for publication and is hence available in [Misc65].

4.1 System model

4.1.1 Node distribution

We consider a square of area ℓ^2 in which network nodes (BSs and UEs) are distributed. The network is assumed to be constrained by the two following invariants :

- a constant total transmit power P_{tot};
- a constant total number of transmit antennas N_a (to be positioned within the network).

The antennas are assumed to be equally distributed on all BSs (whose number N_b is a degree of freedom in the design). Each BS is equipped with $N_{ab} = N_a/N_b$ antennas.

In order to make the location of the BSs realistic, two cases are considered :

- for a small number of BSs $N_b < N_{min}$ (where N_{min} is a threshold that can be arbitrarily chosen), we assume that the BS positions are deterministic and arranged to form a regular grid.
- for a large number of BSs ($N_b > N_{min}$), we assume that the BSs are randomly positioned within the network. The BSs are uniformly distributed one after another, taking into account a repulsion parameter $r_{min} = a\ell/\sqrt{N_b}$ (with $a < 1$). This factor prevents having two BSs too close to each other (i.e. separated by a distance shorter than r_{min}). To sum up, the BSs positions follow a binomial hard core point process.

The number of UEs N_u is supposed to be equal to the total number of transmit antennas N_a. Each UE consists of one receiving antenna. The distribution of the user locations is uniform and follows a binomial point process.

4.1.2 Association and clustering policies

Three different types of environment are considered :

- a fading environment (without large-scale shadowing) in which every channel gain $|h|^2$ follows a complex Gaussian distribution $\mathcal{CN}(0, 1)$;
- an uncorrelated shadowing environment in which every link is obstructed with probability p_o. In this case, $|h|^2 \sim \epsilon\mathcal{CN}(0, 1)$ with $\epsilon \ll 1$ (and $h \sim \mathcal{CN}(0, 1)$ if there is no obstruction).
- a correlated shadowing environment. This scenario features large-scale blockages represented by circular obstacles within the network (see figure 4.1). These circles are generated in two steps. First, their centres are modeled by means of a PPP of intensity λ_o. Afterwards, the radius of each obstacle is determined by sampling a uniform law $\mathcal{U}(0, R_o)$ (where R_o is the maximum possible radius of the obstacles). A link is said to be obstructed if an obstacle lies on the line joining the BS and the UE. The statistical distributions of the channels are the same as the second scenario in the presence or absence of obstruction.

The user association policy is defined as follows.

- For the fading environment, the users are listed and associated to their closest BS one after another. Every BS can serve at most N_{ab} users (since the number of users can at most be equal to the number of antennas). As a result, if its closest BS if already full, a given UE will attempt to connect to its second closest BS, etc.

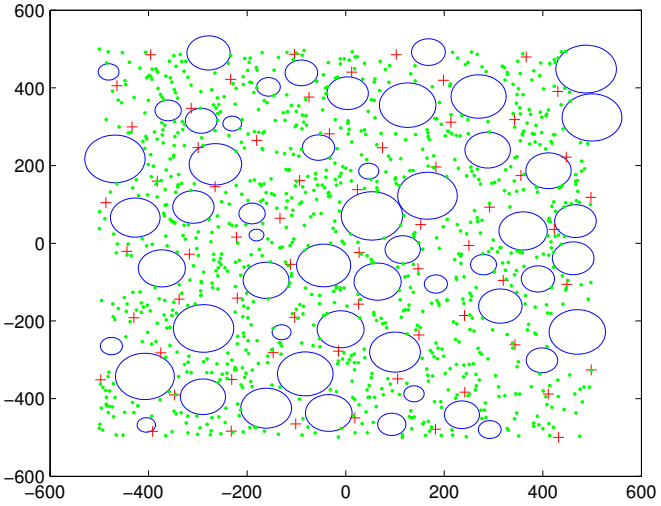

Figure 4.1: Example of network with correlated blockages : the red, green and blue shapes represent BSs, UEs and obstacles respectively.

- For the two shadowing environments, the same rule is applied, except the UEs only connect to the BSs whose link is not obstructed by any obstacle.

Adjacent BSs can later be grouped in order to benefit from cooperative beamforming. We consider here clusters of constant size N_{bc}. Algorithm 1 can be used in that case.

Algorithm 1 Basic clustering algorithm

$N_c = N_b/N_{bc}$ %number of clusters to form
for $i = 0$ to N_c **do**
▷ Select randomly the ith centroid among the BSs that are not part of a cluster yet.
▷ Create the i-th cluster by picking the $N_{bc} - 1$ BSs that are the closest to the i-th centroid (among the BSs still available).
▷ Update the indexes of BSs still waiting to be clustered.
end for

The advantage of this algorithm is that it is computationally inexpensive. However, it is obviously not optimal in terms of association. For instance, the last BSs to be clustered might be very distant from each other. In that case, the users are not separated from their adjacent neighbours (responsible for the highest interference).

4.1.3 Beamforming and normalization

Since each cluster contains N_{bc} BSs, it also includes N_{ac} antennas and serve N_{ac} users, with $N_{ac} = N_{ab}N_{bc}$. A channel matrix $\mathbf{H}_i$ of size $N_{ac} \times N_{ac}$ can therefore be defined for each cluster i.

Let us recall the beamforming techniques analysed here [MIMO30] :

- zero-forcing precoding (ZF) : the objective of this beamformer is to make the users of a cluster orthogonal in order to fully suppress their mutual interference. The precoding matrix $\mathbf{W}_i$ is then expressed as the pseudoinverse of the channel matrix. In our scenario, one can easily observe that the multiplication of $\mathbf{W}_i$ with the channel matrix will produce a diagonal matrix, i.e. that the users of the cluster remain orthogonal, independently of the normalisation.

$$\mathbf{W}_{i,0}^{ZF} = (\mathbf{H}_i^* \mathbf{H}_i)^{-1} \mathbf{H}_i^*. \tag{4.1}$$

- maximum ratio transmission (MRT) : here the objective is to use the beamforming to maximize the useful power received at the UE. In this case, the precoding matrix is classically written as the conjugate transpose of the channel matrix.

$$\mathbf{W}_{i,0}^{MRT} = \mathbf{H}_i^*. \tag{4.2}$$

The beamformers are here constrained to an additional issue: the total transmit power of the system must be equal to the constant P_{tot}. This total power can be expressed as the sum of the squared Frobenius norms of all precoding matrices $\mathbf{W}_i$ $(i = 1, ..., N_c)$:

$$\sum_{i=1}^{N_c} ||\mathbf{W}_i||_F^2 = P_{tot}. \tag{4.3}$$

For the sake of simplicity, one considers here a stronger hypothesis on the power allocation by assuming that P_{tot} is equally distributed between the BSs. The following equation is therefore fulfilled as well.

$$||\mathbf{W}_i||_F^2 = \frac{P_{tot}}{N_c}, \forall i. \tag{4.4}$$

Arguably, sharing the power uniformly is neither realistic nor optimal and it is unnecessary to satisfy (4.3). Using a power control algorithm would be relevant to allocate the powers in an optimal way, but issue will be addressed later in Chapter 5. The constraint can be satisfied by preprocessing the precoding matrices in the following way:

$$\mathbf{W}_i = \frac{\mathbf{W}_{i,0}}{||\mathbf{W}_{i,0}||_F} \sqrt{\frac{P_{tot}}{N_c}}, \tag{4.5}$$

where $\mathbf{W}_{i,0}$ is given by (4.1) or (4.2).

4.1.4 Signal model

Let us define additional notations. In the following, the letters i,j and k respectively represent clusters, UEs and BSs.

- $\mathcal{U}_i$ and $\mathcal{B}_i$, the sets of UEs and BSs indexes associated to cluster i,
- $\mathcal{V}_k$, the sets of UEs associated to BS k,
- d_j, the distance between UE j and the BS to which it is connected,
- d_{jk}, the distance between UE j and an interfering BS k,
- $\mathbf{h}_{ji} \in \mathbb{C}^{1 \times N_{ac}}$, the channel vector between the antennas of cluster i and user j,
- $\mathbf{g}_{jk} \in \mathbb{C}^{1 \times N_{ab}}$, the channel vector between the antennas of BS k and user j,
- $[\mathbf{M}]_{m \in \mathcal{M}}$, a submatrix of $\mathbf{M}$ obtained by extracting the rows whose indexes m belong to the set $\mathcal{M}$,
- σ_j^2, the background noise power affecting user j,
- α, the path loss exponent, taken as constant within the network.

The received power $P_{i^*j^*k^*}$ at a user j^* associated to BS k^* within cluster i^* is expressed in the case of ZF and MRT respectively by :

$$P^{ZF}_{i^*j^*k^*} = \frac{P_{tot}}{N_b||\mathbf{H}^{-1}_{i^*}||^2_F} d^{-\alpha}_{j^*} + \sum_{i\neq i^*}\sum_{k\in\mathcal{B}_i} |\mathbf{g}_{j^*k}[\mathbf{W}_i]_{j\in\mathcal{V}_k}|^2 d^{-\alpha}_{j^*k} + \sigma^2_{j^*}; \tag{4.6}$$

$$\begin{aligned} P^{MRT}_{i^*j^*k^*} = &\frac{P_{tot}|\mathbf{h}_{j^*i^*}\mathbf{h}^*_{j^*i^*}|^2}{N_b||\mathbf{H}^*_{i^*}||^2_F} d^{-\alpha}_{j^*} + \sum_{k\in\mathcal{B}_{i^*}} |\mathbf{g}_{j^*k}[\mathbf{W}_{i^*}]_{j\in\mathcal{V}_k\setminus\{j^*\}}|^2 d^{-\alpha}_{j^*k} \\ &+ \sum_{i\neq i^*}\sum_{k\in\mathcal{B}_i} |\mathbf{g}_{j^*k}[\mathbf{W}_i]_{j\in\mathcal{V}_k}|^2 d^{-\alpha}_{j^*k} + \sigma^2_{j^*}. \end{aligned} \tag{4.7}$$

Note that since $N_a = N_u$, the channel matrices are square. As a result, the pseudoinverse matrix in ZF beamforming is simply a square inverse matrix. This implies that there is no intracluster interference in the case of ZF, unlike the case of MRT.

In both cases, the SINR of the network is equal to the ratio of the first term in equations (4.6) and (4.7) divided by the sum of the other terms.

4.2 Coverage probability analysis

The objective of the following sections is to evaluate the network performance in terms of coverage probability. In the case of a fading environment, several hypotheses related to the model have been assumed to obtain analytical expressions :

- the noise is neglected ($\sigma^2_j = 0\ \forall j$);
- the deterministic and hard core binomial distributions used to position the BSs are approximated by a Poisson Point Process of intensity $\lambda_u = N_u/\ell^2$. The main advantage of this point process is that it approximates the node distribution with a good tradeoff between accuracy and tractability;
- the number of antennas per BS is assumed to be sufficiently large ($N_{ab} \gg 1$);
- the UE is assumed to be connected to its closest BS (this hypothesis is verified for the majority of the users).

Numerical approximations have been performed as well:

- in (4.8), the distribution of the squared Frobenius norm of the inverse channel matrix has been approximated by means of an inverse scaled Chi square distribution of parameters $\frac{\nu}{2}$ and τ^2. Indeed, it can be shown numerically that this distribution fits this squared norm, provided the values of its distribution are adequately selected;
- recent developments have shown that the probability density function (pdf) of the aggregate interference tends to follow an alpha-stable law [SG3], for which no analytical expression is available. This pdf can be either approximated numerically or by using a weighted sum of other distributions.

Based on these approximations, the expressions of proposition 1 can be obtained to estimate the coverage probability.

Proposition 1 : Under the hypotheses of section 4.2, the coverage probability obtained when employing ZF or MRT beamforming can be estimated by the following formulas :

$$P^{ZF}(\theta) = 2\pi\lambda_u \int_{-\infty}^{+\infty} \int_0^{+\infty} \frac{\Gamma(\frac{\nu}{2}; \frac{\nu}{2}\tau^2 N_b \theta i P_{tot}^{-1} r^\alpha)}{\Gamma(\frac{\nu}{2})} f_I(i) r e^{-\lambda_u \pi r^2} dr di; \tag{4.8}$$

$$P^{MRT(\theta)} = \pi\lambda_u \int_{-\infty}^{+\infty} \int_0^{+\infty} \left(1 + \mathrm{erfc}\Big(\frac{P_{tot}(d_{i^*}^\alpha i\theta N_b)^{-1} - 2}{4\sqrt{2N_{ab}}}\Big)\right) f_I(i) r e^{-\lambda_u \pi r^2} dr di. \tag{4.9}$$

In these expressions, $\Gamma(\cdot)$ is the Gamma function and $\Gamma(\cdot;\cdot)$ is the incomplete upper Gamma function.

Proof : in both cases, the coverage probability is defined as :

$$P(\theta) = \mathbb{P}[\mathrm{SIR} > \theta]. \tag{4.10}$$

In the case of MRT, equation (4.16) can be developed using the notations of (4.7) :

$$P(\theta) = \mathbb{P}\left[\frac{P_{tot}|\mathbf{h}_{j^*i^*}|^4 d_{j^*}^{-\alpha}}{N_b||\mathbf{H}_{i^*}^*||_F^2 i_{agg}} > \theta\right]; \tag{4.11}$$

where i_{agg} represents the total aggregate interference received by user j^*. This equation can be rewritten as :

$$P(\theta) = \mathbb{P}\left[\frac{||\mathbf{H}_{i^*}^*||_F^2}{|\mathbf{h}_{j^*i^*}|^4} < \frac{P_{tot}}{N_b d_{j^*}^\alpha i_{agg}}\right]. \tag{4.12}$$

Let us recall that all the entries of $\mathbf{H}_{i^*}^*$ and $\mathbf{h}_{j^*i^*}$ have the same distribution $\mathcal{CN}(0,1)$ since a fading environment is assumed. The following result can be numerically shown :

$$\frac{||\mathbf{H}_{i^*}^*||_F^2}{|\mathbf{h}_{j^*i^*}|^4} \xrightarrow{N_{ab}\gg 1} \mathcal{N}(2, 4\sqrt{N_{ab}}). \tag{4.13}$$

Using the definition of the cdf of a normal distribution, it is possible to rewrite (4.12) :

$$P(\theta) = \mathbb{P}_{i_{agg}, d_{j^*}}\left[\frac{1}{2}\Big(1 + \mathrm{erfc}\Big(\frac{P_{tot}(d_{i^*}^\alpha i\theta N_b)^{-1} - 2}{4\sqrt{2N_{ab}}}\Big)\Big)\right]. \tag{4.14}$$

Let $f_I(i)$ the pdf of the aggregate interference. We will here assume that the UE j^* is associated to its closest BS (this is actually the case for a large majority of the UEs). All the BSs are uniformly distributed within the square of surface ℓ^2. The distribution of the BSs (with is binomial hard core) can be approximated by a PPP of intensity $\lambda_u = N_b/\ell^2$. The two differences of the PPP with the binomial hard core PP are the absence of a repulsion parameter and the variable number of BSs. Under this hypothesis, we can use the pdf $f_R(r)$ of the distance to the closest node of a PPP in R^2 :

$$f_R(r) = 2\pi\lambda_u exp\Big(-\lambda_u \pi r^2\Big). \tag{4.15}$$

This expression can be trivially obtained using the void probability of the two dimensional PPP [SG5]. Averaging (4.14) over i_{agg} and d_{j^*} leads to the expected result.

For the ZF beamforming, one can similarly develop (4.16) by means of equation (4.6) :

$$P(\theta) = \mathbb{P}\left[\frac{P_{tot} d_{j^*}^{-\alpha}}{N_b ||\mathbf{H}_{i^*}^{-1}||_F^2 i_{agg}} > \theta\right]. \tag{4.16}$$

It is possible to numerically observe that $||\mathbf{H}_{i^*}^{-1}||_F^2$ follows a scale inverse Chi square distribution of parameters τ^2 and $\frac{\nu}{2}$. The rest of the proof consists in averaging the cdf of this distribution over i_{agg} and d_j, as for the MRT case.

These analytical estimations are compared in the next section with Monte-Carlo simulations.

4.3 Numerical results

The following setup parameters have been used for all simulations : $\ell^2 = 1$, $\alpha = 3$, $a = 0.8$, $N_{min} = 20$, $P_{tot} = 1$, $N_u = 1024$ and $\sigma_j^2 = 0$ (for all users). In this case, the value of λ_u is thus given by $\lambda_u = N_u/\ell^2 = 1024$.

4.3.1 Fading environment

No clustering

If no clustering is applied, the curves displayed in figure 4.2 suggest the following conclusions.

- Using ZF leads to a higher coverage probability than MRT (for threshold values above 1.5 dB). This observation confirms and generalizes the conclusions of [MIMO30] (whose analysis was restricted to unicellular networks).
- Increasing the number of BSs on which the antennas are distributed increases the coverage as well. In the case of ZF, using a small number of BSs implies that a large number of users are orthogonal with each other. However, the BSs are likely to be on average more distant from their associated users. Even though the interference increases (since less users are orthogonal), the path loss of the useful power is lower with an increased number of BSs, which in total increases the SINR level.
- One can also note that the coverage values are too small to design a realistic and efficient network. Indeed, 80-90 % of users undergo an aggregate interference which is higher than their useful received power. However, this result makes sense since few resources are exploited to separate users. The network can be considered to be fully loaded since all transmissions take place at the same frequency and instant of time. Besides, all the users interfere with each other except if they are connected to the same BS. In the following paragraph, we cluster the BSs in order to make more UEs orthogonal.

Comparison with approximate formulas

Figure 4.3 displays an example of comparison between the estimation formulas and Monte Carlo simulations. The curves do not superimpose each other exactly due to the hypotheses used to derive the formulas. Nevertheless, the estimation remains fairly accurate.

Clustering

Figure 4.4 illustrates the coverage for several cluster sizes. One can note MRT beamforming now produces higher values on average. Indeed, increasing the number of cooperating BSs enables to separate more users in case of ZF. However, BSs of a larger cluster are on average located at a higher distance from the user and cause potentially less interference. By contrast, the

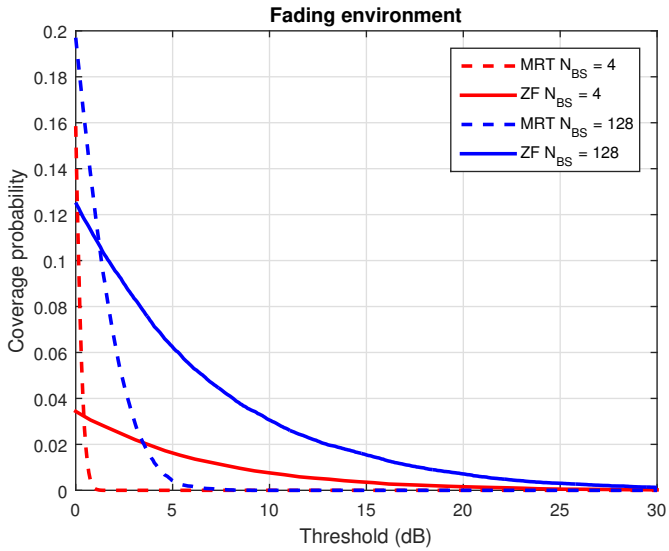

Figure 4.2: Comparaison of ZF and MRT for a fading environment (with no clustering).

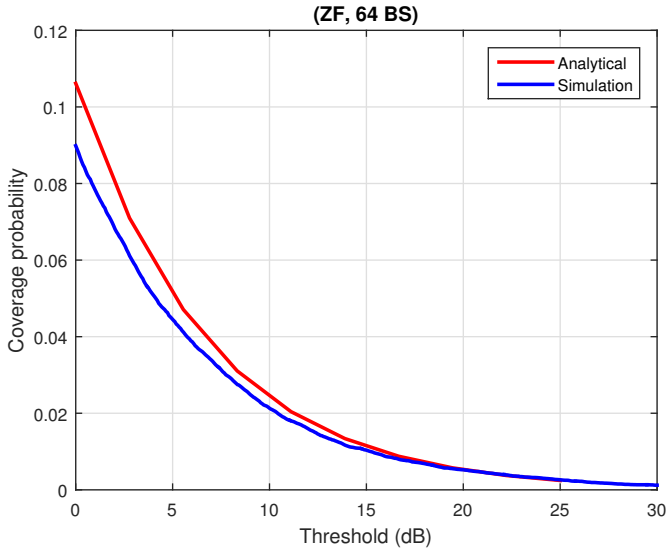

Figure 4.3: Comparison of analytical and numerical results in the case of ZF beamforming with no clustering and $N_b = 64$.

MRT beamformers can collect power from more antennas when increasing the cluster size. As a consequence, the useful power significantly increases. The numerical simulations confirm this justification : the increase in useful power with MRT is larger than the decrease in interference when employing ZF.

4.3.2 Environment with uncorrelated shadowing

Incorporating blockages within the model implies the following consequences:

- the user association policy changes. A given UE equipment may not connect to its closest BS if its link is obstructed. In that case, the useful power is lower owing to a higher path loss (since the associated BS of the UE is further away). It might also happen that all the links of a given user are obstructed. The user then attempts to connect to the closest BS which is not full (using the same policy as for the fading environement);

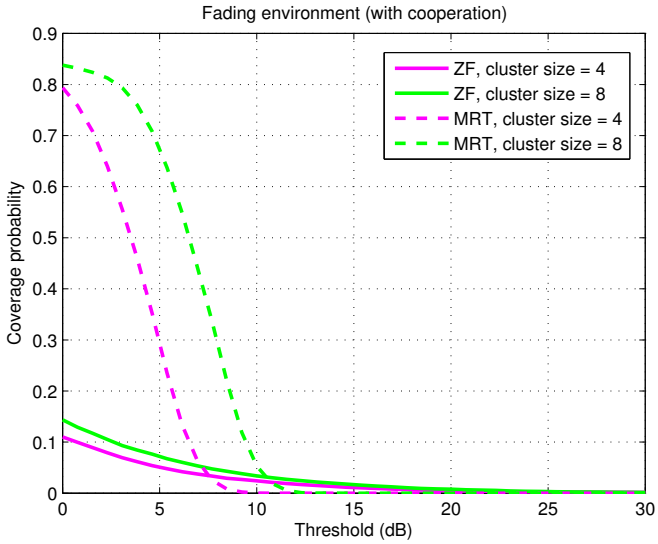

Figure 4.4: Comparaison of ZF and MRT for a fading environment with $N_b = 64$ and a cluster size of 4 or 8.

- since the users are associated with their respective BSs in successive order, the last users to be connected may even be forced to receive their useful signal from an obstructed BS;
- the aggregate interference is lower on average since several interfering links are obstructed.

Figure 4.5 compares the coverage of the fading environment (for which $p_o = 0$) with the uncorrelated shadowing environment for $p_o = 0.4$ or 0.7.

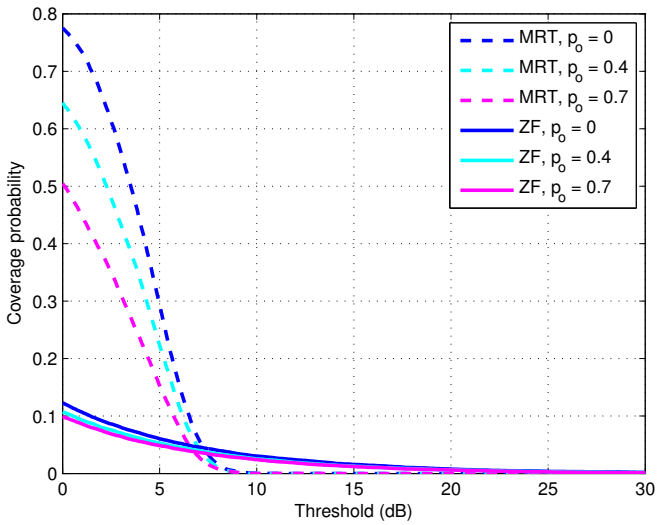

Figure 4.5: Comparaison of ZF and MRT for a different environments with $N_b = 64$ and a cluster size of 4.

One can observe that the coverage probability decreases for both ZF and MRT when the probability p_o increases (i.e. when more links are obstructed). This means that the useful received signals are attenuated by a larger factor than the decrease in interference.

The higher average path loss is not the main cause of this decrease in the useful power :

- For the MRT beamforming, the useful power of users belonging to cluster i is proportional

to the square of the diagonal elements of matrix $\mathbf{H}_i\mathbf{W}_i$. If more obstacles are included in the network, more entries of $\mathbf{H}_i$ will be attenuated by the factor ϵ. As a consequence, the resulting values of the matrix product with $\mathbf{W}_i$ are lower;

- For the ZF beamforming, the matrix product $\mathbf{H}_i\mathbf{W}_i$ produces a diagonal matrix whose diagonal entries are all equal to $1/||\mathbf{H}_i^{-1}||_F$. When the values of p_o increases, more entries of H_i are likely to be attenuated by the factor ϵ. In that case, numerical simulations have shown that the norm of the inverse channel matrix $||\mathbf{H}_i^{-1}||_F$ increases on average. This statistical change in the normalization factor results in a decrease in the useful power.

4.3.3 Environment with correlated shadowing

In case of correlated shadowing, the obstacle density is characterized by the parameters λ_o and R_o defined in Section 2. Figure 4.6 compares the coverage in the fading environment ($R_o = \lambda_o = 0$) with the shadowing environment for two pairs of values of λ_o and R_o. These values have been chosen to produce the same percentage of obstructed links as in figure 4.5 (i.e. an equivalent probability p_o equal to 0.4 or 0.7).

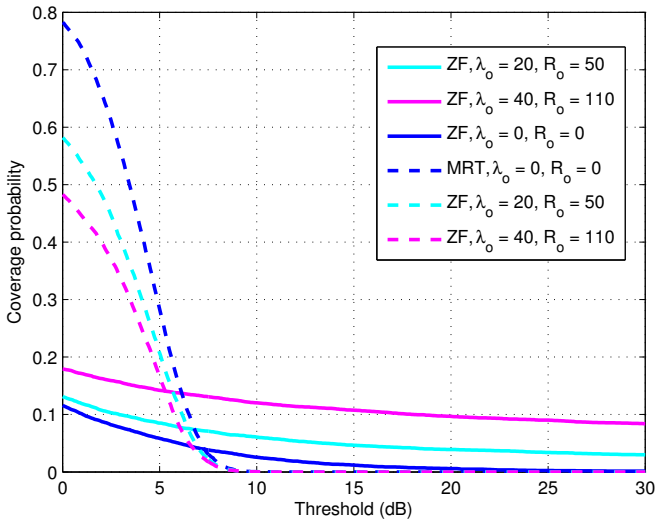

Figure 4.6: Comparaison of ZF and MRT for a correlated shadowing environment with $N_b = 64$ and a cluster size of 4.

Regarding the MRT beamforming, the results are the same as for the environment with uncorrelated shadowing. However, for the ZF beamforming, the coverage now increases with the density of obstacles. This divergence with the case of uncorrelated shadowing is due to the statistics of fully obstructed users. The number of fully obstructed users actually tends to zero for the uncorrelated shadowing scenario. By contrast, for the correlated shadowing, this number tends to follow a distribution with a non-zero mean. To summarize, for a same percentage of obstructed links, they are statistically more fully obstructed users in the case of correlated shadowing. These users undergo very little interference (compared the other users) since all their interfering links are obstructed. Besides, their useful power is higher on average as well. This is again due to the normalization factor $1/||\mathbf{H}_i^{-1}||_F$. All the entries of the channel matrix of these users are attenuated by the factor ϵ, resulting in a significantly lower value of $|\mathbf{H}_i^{-1}||_F$ on average compared to the other users. This property has been numerically verified.

4.3.4 Influence of the number of transmit antennas

In the previous sections, the number of transmit antennas N_a has been equal to the number of users N_u. However, MU-MIMO models often assume that $N_a \gg N_u$ [PC47]. Hence, we now evaluate the impact of deploying several transmit antennas per user (but still with the same total transmit power P_{tot}). Figure 4.7 displays the coverage for several values of the number of antennas per user N_{au}.

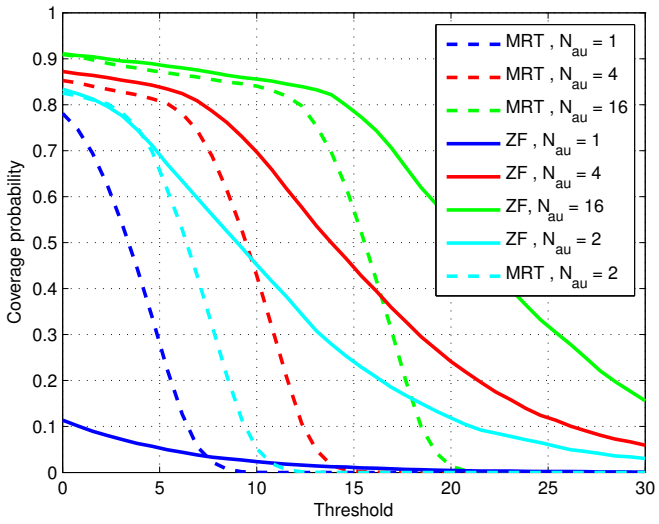

Figure 4.7: Comparison of ZF and MRT in a fading environment for several values of N_{au}, $N_b = 64$ and a cluster size of 4.

As expected, the coverage significantly increases with the number of antennas per user. One can observe that the ZF beamforming is now more efficient than MRT when $N_{au} > 1$. The results are shown for a fading environment but the conclusions are identical for the two shadowing environments. Thanks to this increase in the number of antennas, the order of magnitude of the SIR level is now similar to values measured in practical networks (15 dB of SIR is often considered to be satisfactory, see [Misc60]).

4.3.5 Influence of the noise power

Figure 4.8 displays the coverage probability of the network (expressed in terms of SINR) for several values of the background noise power. This noise is assumed to be constant on all links and has been computed to obtain a mean SNR of 5, 15 and 25 dB. One can observe the decrease in the coverage when selecting higher values for σ^2.

4.4 Optimal clustering method

We now propose a method to improve the clustering of the BSs. We first present an approach to optimize the cluster size by using the notion of spectral efficiency. Then, we detail an algorithm enabling to group the BSs more efficiently than algorithm 1.

4.4.1 Optimal cluster size

The strategy developed in this section is inspired from [MIMO25] and consists in selecting the cluster size that numerically maximizes the spectral efficiency. Let us recall the definition of this metric :

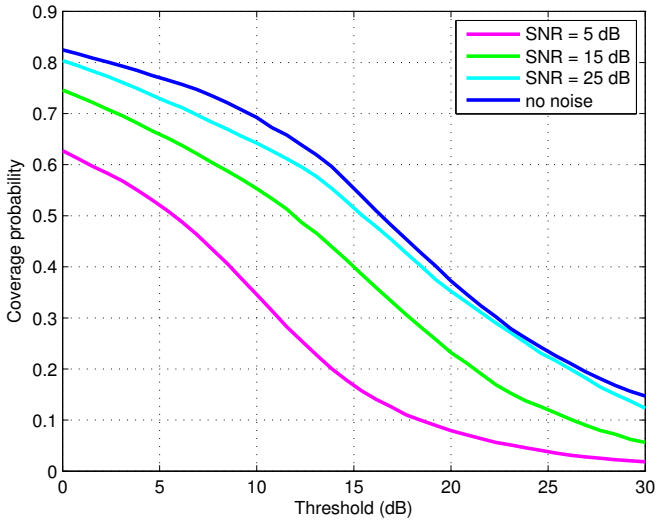

Figure 4.8: Coverage probability computed for several SNR values, with $N_{au} = 12$, $N_b = 64$, ZF beamforming, a correlated environment (with $\lambda_o = 25$ and $R_o = 100$) and a cluster size of 4.

$$C = \mathbb{E}\big[\log(1 + \text{SINR})\big] = \int_0^{+\infty} \log(1 + \text{SINR})\, d(\text{SINR}). \tag{4.17}$$

This definition does however not include the pilot overhead needed to exchange CSI between BSs of the same cluster. These pilot symbols need to be transmitted every time the channel significantly changes. In a static channel, the CSI will be exchanged less regularly than in a channel whose impulse response change more rapidly. Let us define the fading coherence L_b as the number of symbols (including pilots) that can be transmitted before needing to update CSI and hence to transmit a new sequence of pilots. Let L_p, the number of symbols dedicated to pilots. This number depends in general on the SNR, the number of antenna per BS N_{ab}, and the cluster size N_{bc}. We here model L_p as $L_p = \eta N_{ab} N_{bc}$, where $\eta \geq 1$ is a parameter that depends on the SNR [MIMO35]. The (relative) overhead can be defined as :

$$\beta = \frac{L_p}{L_b} = \frac{\eta N_{ab} N_{bc}}{L_b}. \tag{4.18}$$

The effective spectral efficiency can hence be defined as :

$$C_{eff} = (1 - \beta)\, C. \tag{4.19}$$

In this expression, both β and C depend on the cluster size N_{bc}. Indeed, C depends on the SINR distribution which depends itself on N_{bc}. The cluster size can hence be selected in order to maximize this effective spectral efficiency :

$$N_{bc}^* = \text{argmax}_{N_{bc} \in \mathbb{N}}\, C_{eff}\Big(\beta(N_{bc}), \text{SINR}(N_{bc})\Big). \tag{4.20}$$

Figure 4.9 displays the effective spectral efficiency as function of the cluster size for several values of L_b. The following parameters have been chosen : $N_b = 120$, $N_u = 240$, $N_{au} = 2$, $\lambda_o = 25$, $R_o = 100$ and $\epsilon = -30dB$. The noise power has been chosen in order to result in a SNR of 25 dB when $N_{bc} = 1$. Since this SNR value corresponds to relatively good conditions for practical networks [Misc59], we here assume that η is equal to 1 [MIMO25].

One can note that the value of the optimal cluster size increases with the coherence length. This observation makes sense since the BSs can in that case afford exchanging more pilots for the same value of β.

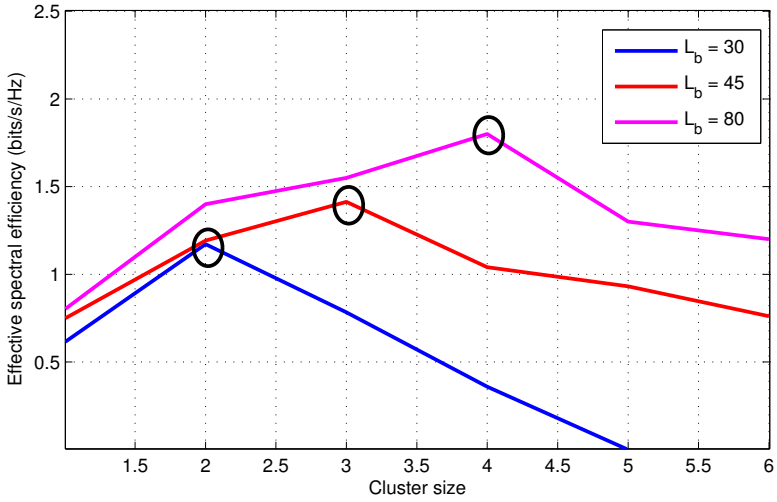

Figure 4.9: Effective spectral efficiency as function of the cluster size, parametrized by L_b (the maxima are circled in black).

4.4.2 Improved clustering algorithm

As mentioned in section 4.1.2, algorithm 1 is not optimal since the last clustered BSs might not be adjacent (see figure 4.10).

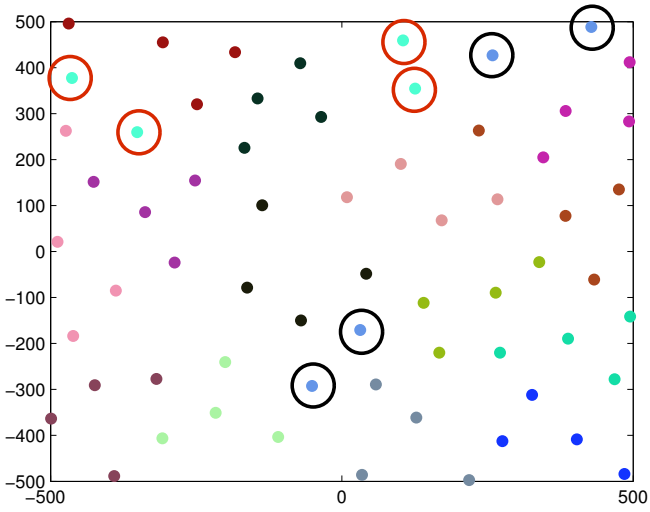

Figure 4.10: Clusters obtained using algorithm 1. Points of the same color represent BSs assigned to the same cluster. The circled points represents the lasts cluster that have been formed.

The coverage of these last clusters is displayed in figure 4.4.2. One can observe that their values are lower than the average coverage of the network. The users associated to these clusters undergo more interference due to their neighboring BSs that are associated to other clusters.

Algorithm 2 can be used to overcome this drawback. The first part of this algorithm clusters the BSs located nearby the corner or edges of the network. As seen in figure 4.10, these BSs are likely to be badly clustered when using algorithm 1. To avoid this problem, they are now clustered in the first place. The rest of the algorithm is an adaptation from the content of [Misc61]. The iterations do not stop until the maximum distance between two intra-cluster BSs is below a

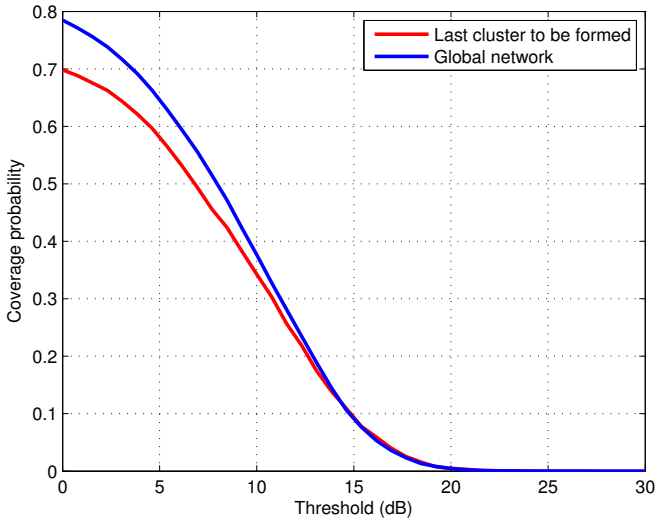

Figure 4.11: Comparison of the global coverage with the coverage of the last clusters to be formed using algorithm 1. The values have been obtained for a fading environment, MRT beamforming, $N_b = 64$ and $N_{bc} = 4$

.

certain threshold. This condition is used to make sure that all intra-cluster BSs are neighbors with a high probability.

As seen in the example in figure 4.12, all the clusters former now contain adjacent BSs exclusively.

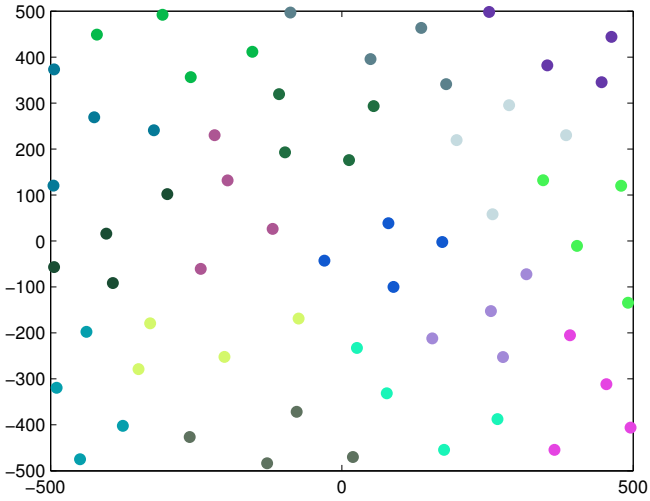

Figure 4.12: Example of clusters formed using algorithm 2 with $N_b = 64$ and $N_bc = 4$. One can note that the issue in figure 4.10 is no longer present.

Algorithm 2 Advanced clustering algorithm

▷ Compute the optimal cluster size N_{bc} using the method of section 4.4.1;
▷ Compute the number of clusters to form $N_c = N_b/N_{bc}$;
▷ Detect the BSs that are close to the corners and edges of the square delimiting the network;
▷ Cluster these BSs using algorithm 1 (by setting as them as centroids and by using other adjacent BSs if necessary);
% The rest of the algorithm is used to cluster the remaining BSs.
▷ Define d_{min}, the maximum desired distance between BS of the same cluster;
▷ Set $d = +\infty$;
while $(d > d_{min})$ **do**
▷ Initialize the centroids by selecting them between the remaining BSs uniformly (or using Kmeans++ [Misc66]);
    while all the BSs are not yet assigned to a cluster **do**
        ▷ Sort the BSs by the distance to their closest centroid minus distance to the farthest centroid;
        ▷ Assign BSs (in the order defined at the previous step) to their closest cluster until a cluster is full.
        ▷Resort the remaining BSs, without taking the full clusters into account;
    end while
    while transfers need to be performed **do**
        Compute current cluster means to define new centroids;
        ▷ For each BS, compute the distances to all the centroids;
        ▷ Sort BSs using the difference between the current assignment and the best possible ; alternate assignment
        for each BS (whose order of determined by the previous step) **do**
            for each cluster **do**
                ▷ If there is a BS willing to leave anoter other cluster and this swap yields and improvement, swap the two BS;
            end for
        end for
    end while
    ▷ Compute d, the maximum intra-cluster distance of the network;
end while

Chapter 5

Power control algorithms

In this chapter, we consider strategies to allocate transmit powers in the MIMO networks previously developed. Indeed, the models of chapter 4 assume a constant transmit power for all antennas, resulting in the loss of one degree of freedom that could improve the network performance. We now investigate how the network can benefit from a variable power allocation. The three PC algorithms detailed in this chapter are summarized here below.

The Min-Max algorithm is used to improve the coverage probability of the network [PC44]. This method is particularly useful in the case of a static channel. Indeed, it enables to improve the QoS of users who could initially not be served due to their low SINR values (e.g. cell-edge users).

The water filling algorithm is introduced in [PC42] and can be employed in scenarios where the channel impulse responses change pretty rapidly over time. In such environments, most users are guaranteed to be in sufficiently good channel conditions within a reasonable amount of time. In other words, all the users do not have a good QoS at the same instant but are ensured to be served within a relatively short time interval. In terms of power allocation, it is not necessary to help users in bad channel conditions since their SINR values will increase in the short term. It is hence more relevant to allocate powers over the users in good condition in order to increase their respective spectral efficiencies.

The last method proposes a joint optimization of the beamformers and the power allocation at the level of the entire network [PC45]. Thanks to this global approach, the coverage probability reaches higher values than those obtained by computing the beamformers and by applying the Min-Max algorithm separately. However, the algorithm is characterized by a very low computational efficiency and might not be applicable in practical settings.

It is important to emphasize that these algorithms should not be compared in a direct manner : as mentioned above, they are valid for rather different scenarios. Besides, due to space constraints, the analysis is restricted to these three methods. Many other algorithms are of course available in the literature and might be applicable to the proposed network model. The reader is referred to [PC41] for an overview of the existing methods. The three proposed techniques have been selected due to their differences and because they feature interesting mathematical backgrounds and interpretations.

5.1 The Max-Min algorithm

5.1.1 Theoretical background

We consider the same downlink scenario as in chapter 4 : N_u users are served simultaneously (using the same time and frequency resources) and have different SINR levels SINR_i ($i = 1, ..., N_u$). The total available transmit power for all the BSs is given by P_{tot}. The Max-Min algorithm aims at improving the SINR values in such a way to maximize the minimum SINR value that can be observed among the UEs. This approach is followed in [PC44] and can be formulated in terms of the following optimization problem :

$$\begin{aligned} \text{maximize} \quad & \min_i \gamma_i \\ \text{subject to} \quad & \text{SINR}_i(p_i) \geq \gamma_i \ \forall i \\ & \sum_{i=1}^{N_u} p_i = P_{tot}. \\ \text{variables} \quad & p_i, \ \gamma_i \ \forall i \end{aligned} \tag{5.1}$$

In this formulation, γ_i is the target SINR value to be reached at user i and is here considered as an optimization variable (in other words, its value its not fixed in advance). We also introduce the symbol p_i which denotes the allocated transmit power to serve user i.

Regarding our MIMO network, it is now necessary to allocate different powers for users associated to the same BS. Hence, the normalisation of the precoding matrices can no longer be performed as in (4.5). We now proceed in three steps to do the normalization :

- every column of the precoding matrix $\mathbf{W} \in \mathbb{C}^{N_{ac} \times N_{uc}}$ is separately normalized.
- the matrix is divided by $\sqrt{N_{uc}}$ in order to have a unitary Frobenius norm.
- finally, the powers are allocated by multiplying every column of the precoding matrix by the square root of the power allocated for its associated user.

One can easily observe that this normalization does not change the properties of the ZF beamforming (orthogonality of users) nor the MRT beamforming (maximum useful power).

For sake of simplicity, we will define an effective gain matrix $\mathbf{G} \in \mathbb{R}^{N_u \times N_u}$ whose entry G_{ij} represents the gain (in terms of power) of user i with respect to the symbol intended to user j. This gain includes the path loss, the beamforming and the fading channel. Using this definition, it is possible to redefine the SINR of user i in the following way :

$$\text{SINR}_i = \frac{G_{ii} p_i}{\sum_i G_{ij} p_j + \sigma_i^2}, \tag{5.2}$$

where σ_i^2 is the background noise power affecting user i. As mentioned in [PC44], the problem can be rewritten in a linear form by introducing the auxiliary variable t :

$$\begin{aligned} \underset{t \geq 0}{\text{maximize}} \quad & t \\ \text{subject to} \quad & \sum_{j \neq i} G_{ij} p_j - G_{ii} p_i + \sigma_i^2 \leq t; \forall i \\ & \sum_{i=1}^{N_u} p_i = P_{tot}. \\ \text{variables} \quad & p_i, \forall i \end{aligned} \tag{5.3}$$

It is hence possible to show (using linear optimization theory) that the constraints of (5.3) will be tight at the optimum. This means that all the SINRs at the optimum will be equal to the target SINR t. It is possible to solve the problem in centralized manner : since the constraints regarding the SINR are all tight, they can be rewritten to form a matrix equation. Solving this matrix equation will produce the optimal values of the SINR and the powers to allocate. Since the network may contain many users, inverting this equation might require a lot of computation time. Besides, once the optimal powers are determined, it would be necessary to communicate their values to their respective BSs via backhaul links, which might not be very practical.

Another option is to solve problem (5.3) iteratively, thanks to algorithm 3. This algorithm is characterized by a convergence condition that can be derived thanks to Perron-Frobenius theorem [PC41]. If this condition is satisfied, it is possible to show that the iterations performed in algorithm 2 are equivalent to solving problem (5.3) [PC46]. Let us introduce two additional matrices $\mathbf{D}$ and $\mathbf{F}$, defined as follows :

$$\mathbf{D} = \gamma \mathbf{I}_{N_u} \text{ (where } \mathbf{I}_n \text{ is the identity matrix of size n) ;}$$

$$F_{ij} = \begin{cases} 0 & \text{i=j} \\ \mathrm{G}_{ij}/G_{ii} & \text{i} \neq j \end{cases}$$

Algorithm 3 converges iff the spectral radius of the matrix product of $\mathbf{D}$ and $\mathbf{F}$, $\rho(\mathbf{DF})$ is lower than one.

5.1.2 Implementation

A distributed implementation of the Max-Min algorithm is proposed below :

Algorithm 3 Distributed Max-Min algorithm

▷ Set the threshold value ϵ and the update values δ and α;
▷ Set a stopping criterion for the power updates (e.g. maximal number of iterations);
▷ Set an initial value for γ;
% 1 - Determine the optimal value of γ to have convergence.
▷ Compute matrices $\mathbf{D}$ and $\mathbf{F}$;
while $(\rho(\mathbf{DF}) > 1)$ or $(\rho(\mathbf{DF}) < 1 - \epsilon)$ **do**
  if $(\rho(\mathbf{DF}) > 1)$ **then**
    $\gamma \leftarrow (1 - \delta)\gamma$;
  end if
  if $(\rho(\mathbf{DF}) < 1 - \epsilon)$ **then**
    $\gamma \leftarrow (1 + \delta)\gamma$;
  end if
end while
% 2 - Determine the values of the powers to allocate
while $\Big($(powers not yet allocated) or $(\sum_i p_i > P_{tot})\Big)$ **do**
  $p_i(0) \leftarrow 1/N_u \ \forall$ user i ; % initialize the powers
  while (stopping criterion not fulfilled) **do**
    $p_i(t+1) \leftarrow \frac{\gamma}{\mathrm{SINR}_i(t)} p_i(t), \ \forall \ i;$
  end while
  if $(\sum_i p_i > P_{tot})$ **then**
    $\gamma \leftarrow (1 - \alpha)\gamma;$
  end if
end while

5.1.3 Simulation results

The algorithm has been tested in a fading environment, for the following parameters : $N_b = 16$, $N_u = 128$, $N_{bc} = 1$, $N_{au} = 32$ and a mean SNR of 10 dB. Figure 5.1 displays the network coverage before and after applying the Max-Min algorithm. Looking at the green curve, one can observe that approximately 10 % of the users experience a negative SINR (expressed in dB). The value of their useful power is thus lower than their received corrupting power. These users are hence not in a position to be efficiently served. After applying the algorithm, the SINR values are all concentrated around 11 dB, which is a typical SINR values in realistic networks [Misc60]. As a conclusion, all the users can now be served thanks to the algorithm.

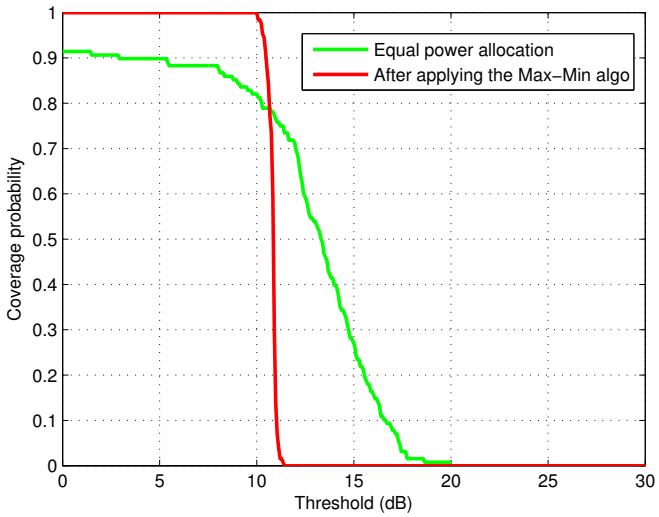

Figure 5.1: Coverage probability of the network before and after applying the Max-Min algorithm.

5.1.4 Comments

The advantage of this algorithm is that it can be executed in a distributed manner. Indeed, once the target SINR value has been determined, the main remaining operation is the iteration $p_i(t+1) = \frac{\gamma}{\mathrm{SINR}(t)_i} p_i(t)$. This operation can be performed individually by each BS for the users i that are associated with it. As a result, no exchange of information is required between the BSs. The algorithm can actually be interpreted as a non-cooperative game (see [PC46] for more details).

The algorithm however suffers from one main limitation. The final value of the SINR might not be as high as desired. For instance, if another set of parameters is used in the above example, the resulting value of the SINR might be of 1 or 0 dB, which is not possible for a realistic network to operate. This might be due to the channel gains (which directly influence the maximum possible target SINR via the condition $\rho(\mathbf{DF}) < 1$ and/or the noise power (which might decrease the target SINR value during the algorithm). In such cases, the algorithm attempts to improve the coverage of a too large number of users in bad conditions. A solution might be to apply the algorithm on a subset of the users, excluding users that are in too bad conditions to be served (even if PC is employed).

5.2 The iterative water filling algorithm

5.2.1 Theoretical background

As mentioned in the introduction, the role of the iterative water filling algorithm is not to improve the coverage but the spectral efficiency (also named capacity). The channel is supposed to change quickly over time. Hence, users in a bad condition at a given instant are likely to benefit from better channel gains in the short term. Let us recall the definition of the spectral efficiency :

$$C = \sum_{i=1}^{N_u} log(1 + \mathrm{SINR}_i). \tag{5.4}$$

The objective of the iterative water filling algorithm is to solve the following optimization problem :

$$\begin{aligned} &\text{maximize} && C \\ &\text{subject to} && \sum_{i=1}^{N_u} p_i = P_{tot}. \\ &\text{variables} && p_i,\ \forall i \end{aligned} \tag{5.5}$$

Like the Max-Min algorithm, this problem can be viewed as a non-cooperative game. The uniqueness of a Nash equilibrium for this game is proved in [PC42]. The best response strategy for each user is derived in the same paper. At every iteration, all the users should update their transmit powers by performing the same update operation :

$$p_i(t+1) = max\Big(\mu - c_i(t), 0\Big). \tag{5.6}$$

where μ is a positive constant satisfying the power constraint of (5.5) and the coefficients c_i are defined as :

$$c_i(t) = \frac{\sum_{j \neq i} G_{ij} p_j(t) + \sigma_i^2}{G_{ii}}. \tag{5.7}$$

5.2.2 Implementation

Algorithm 4 Iterative water filling algorithm

▷ Set an initial value for μ and the update factor δ and ϵ;
▷ Set a stopping criterion (e.g. a maximal number of iterations);
▷ Set an initial value for the powers : $p_i(0) \leftarrow 1/N_u$, $\forall i$;
while $\Big($(powers not yet allocated) or $(\sum_i p_i > P_{tot}$) or $(\sum_i p_i < P_{tot}$ - $\epsilon)\Big)$ **do**
  while (stopping criterion not fulfilled) **do**
    ▷ Update the interference coefficients $c_i(t) \leftarrow \Big(\sum_{j \neq i} G_{ij} p_j(t) + \sigma_i^2\Big)/G_{ii}$, $\forall i$;
    ▷ Update the powers $p_i(t+1) \leftarrow max\Big(\mu - c_i(t), 0\Big)$, $\forall i$;
  end while
  if $(\sum_i p_i > P_{tot})$ **then**
    $\mu \leftarrow (1 - \delta)\mu$;
  end if
  if $(\sum_i p_i < P_{tot} - \epsilon)$ **then**
    $\mu \leftarrow (1 + \delta)\mu$;
  end if
end while

5.2.3 Simulation results

The algorithm has been applied on the same example as section 5.1.3 (with the same set of parameters). The allocated powers are displayed in figure 5.2. The dark plot represents the coefficients c_i accounting for the interference and the noise affecting each user. One can observe that the algorithm performs the expected result. The blue plot represents the allocated powers that are computed using (5.6). The value of the coefficient μ can be deduced by reading the horizontal height reached by the powers (0.019 here). One can also note that no power has been given for users in too bad conditions (i.e. whose coefficient c_i exceeds the water level). As expected, the spectral efficiency obtained after the use of this algorithm is higher than if the Max-Min algorithm is applied.

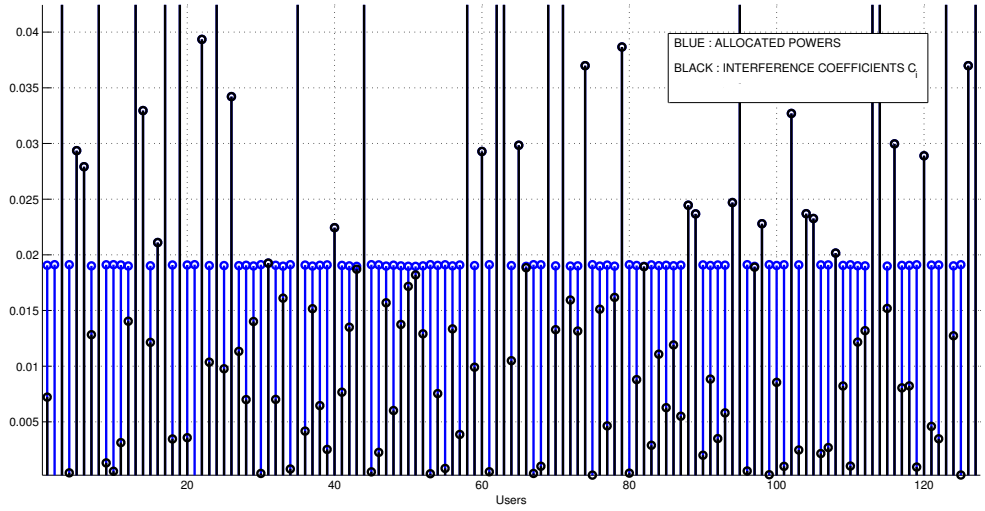

Figure 5.2: Allocated power and interference coefficients after applying the water filling algorithm. Each horizontal index represents a user of the network.

5.3 Joint power control and beamforming

5.3.1 Mathematical background

In this section, a last algorithm initially proposed in [PC45] is explained in detail. Its implementation is rather different from the previous methods for two main reasons. Firstly, the algorithm computes both beamformers and power allocation simultaneously. This was not the case for the Max-Min and waterfilling algorithms for which the power allocation was performed after the beamforming (MRT or ZF). Secondly, the operations of this new method have to be performed in a centralized manner. This means that the algorithm can neither be distributed, nor be modeled by a non-cooperative game. Another consequence is the significant computational cost. Owing to the joint approach, the channels of all network links must be known simultaneously, implying a lot of overhead due to CSI exchange. Besides, the mathematical operations are themselves more complex as they involve matrices of larger sizes.

The objective of the algorithm can again be formulated as an optimization problem [PC45] :

$$\begin{aligned} \text{maximize} \quad & \min_i \gamma_i \\ \text{subject to} \quad & \text{SINR}_i(\mathbf{W}, \mathbf{p}) \geq \gamma_i \ \forall i \\ & \sum_{i=1}^{N_u} p_i = P_{tot} \\ & ||\mathbf{w}_i||_2 = \sqrt{1/N_u} \ \forall i, \\ \text{variables} \quad & \mathbf{W}, \mathbf{p}, \boldsymbol{\gamma}, \end{aligned} \tag{5.8}$$

where $\mathbf{W} \in \mathbb{C}^{N_a \times N_u}$ represents the precoding matrix of the global network (i.e. the beamformers of all the BSs cooperating as one unique cluster) and $\mathbf{w}_i$ represents the ith column of $\mathbf{W}$ (beamforming vector associated to the ith user). The vectors $\mathbf{p}$ and $\boldsymbol{\gamma}$ respectively contain the powers p_i and SINR levels γ_i of all users i.

Let $\mathbf{h}_i \in \mathbb{C}^{N_a \times 1}$, the channel between all the antennas of the network and user i. The components of this vector include here both fading and path loss. One can also define a coupling matrix $\boldsymbol{\Phi}(\mathbf{W}) \in \mathbb{C}^{N_u \times N_u}$ and an equivalent noise $\boldsymbol{\eta}(\mathbf{W})$ in the following way :

$$\boldsymbol{\Phi}_{ij} = \begin{cases} 0 & \text{i=j} \\ |\text{w}_i^T \mathbf{h}_j|^2 / |\mathbf{w}_i^T \mathbf{h}_i|^2 & \text{i} \neq j \end{cases}$$

$$\boldsymbol{\eta}_i(\mathbf{W}) = \frac{||\mathbf{w}_i||_2^2}{|\mathbf{w}_i^T \mathbf{h}_i|^2} \sigma_i^2. \tag{5.9}$$

where σ_i^2 is the background noise power affecting user i.

The algorithms relies on two results mentioned in [PC41] and [PC45] :

- Given the precoding matrix $\mathbf{W}$, the optimal target SINR γ^* and the optimum powers $\mathbf{p}^*$ can be obtained by computing the extended coupling matrix $\mathbf{G}_{ex} \in \mathbb{C}^{(N_u+1)\times(N_u+1)}$, defined as follows :

$$\mathbf{G_{ex}} = \begin{pmatrix} \mathbf{D}(\boldsymbol{\gamma})\boldsymbol{\Phi}^{\mathbf{T}}(\mathbf{W}) & \mathbf{D}(\boldsymbol{\gamma})\boldsymbol{\eta}(\mathbf{W}) \\ \frac{1}{P_{tot}} \mathbb{1}^T \mathbf{D}(\boldsymbol{\gamma})\boldsymbol{\Phi}^{\mathbf{T}}(\mathbf{W}) & \frac{1}{P_{tot}} \mathbb{1}^T \mathbf{D}(\boldsymbol{\gamma})\boldsymbol{\eta}(\mathbf{W}) \end{pmatrix} \tag{5.10}$$

  where $\mathbb{1}$ is the vector of length N_u whose entries are all equal to 1. The spectrum of this matrix has several interesting properties. Its largest eigenvalue is strictly positive and is equal to the inverse of γ^*, the optimal target SINR value. It can be proven that this optimal value is the same for all the users (in other words, $\boldsymbol{\gamma}^* = \gamma^* \mathbb{1}$). Furthermore, the eigenvector associated with this eigenvalue is equal to $[1 \ \mathbf{p}^{*T}]^T$.

- Given fixed allocated powers $\mathbf{p}$, the optimum beamforming vector $\mathbf{w}_i^*$ is given by :

$$\mathbf{w}_i^* = \left(\sum_{j \neq i} p_j \mathbf{h}_i \mathbf{h}_j^H + \sigma_i^2 \mathbf{I}_{N_a} \right)^{\dagger} \mathbf{h}_i. \tag{5.11}$$

5.3.2 Implementation

Thanks to above results, one can define the algorithm below by optimizing the beamforming and the power allocation alternately [PC41].

Algorithm 5 Joint beamforming and power allocation

▷ Select a stopping criterion (e.g. a maximum number of iterations)
while (stopping criterion not fulfilled) **do**
  ▷ Compute the beamformers $\mathbf{w}_i$ using (5.11);
  ▷ Compute the extended coupling matrix $\mathbf{G}_{ex}$ using (5.10);
  ▷ Compute the largest eigenvalue λ_{max} of $\mathbf{G}_{ex}$ and its associated eigenvector $\mathbf{v}_{max}$.;
  ▷ Compute the optimal target SINR $\gamma^* \leftarrow \lambda_{max}^{-1}$;
  ▷ Compute the optimal powers $\mathbf{p}^* \leftarrow \mathbf{v}_{max}[2 : N_u]$;
end while

5.3.3 Simulation results

The algorithm has been tested in a fading environment for $N_b = 4$, $N_u = 32$, $N_{bc} = 4$, $N_{au} = 4$ and a mean SNR of 10 dB. The obtained coverage is displayed in figure 5.3. The results are compared with same network and the same noise power using ZF beamforming folllowed by the Max-Min PC algorithm. As expected, one can observe that the joint optimization yields better performance. Indeed, the beamformers obtained in the joint approach are computed in eq. (5.11) to optimize the SINR. Both interference and noise are hence taken into account. By contrast, the ZF beamformers are computed to make users orthogonal and do not take the noise power into account.

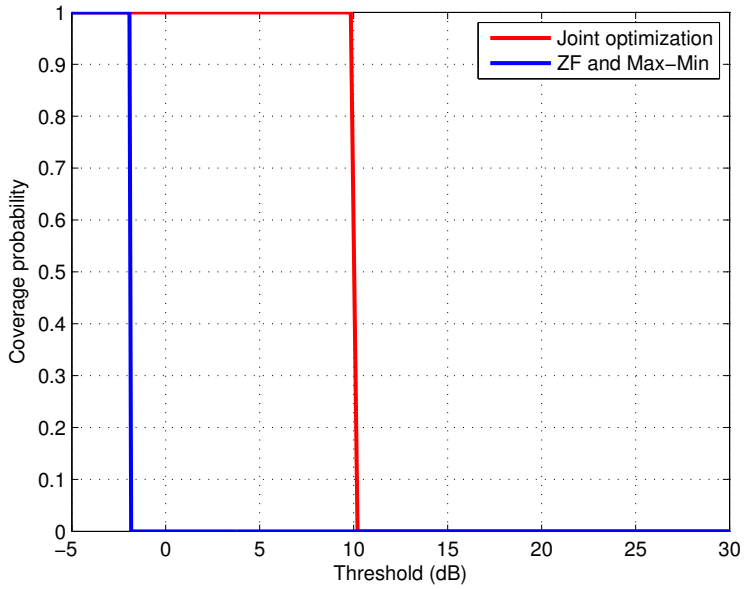

Figure 5.3: Comparison of the joint optimization algorithm with the Max-Min algorithm used after applying ZF beamforming.

Chapter 6

Analysis of a heterogeneous network

This chapter is based on two objectives : on the one hand, gathering all the concepts introduced so far within a single model and on the other hand, introducing the notion of heterogeneous network. With this aim in view, we propose a large scale model including these features.

It is important to note that this last network must be considered as a test case. Regarding the heterogeneous aspect, we hence do not provide a complete analysis of general K-tier networks. In addition to summarizing the notions of this thesis, the role of this model is rather to identify their limits and to introduce elements that should be taken into account for a potential generalization to HetNets.

6.1 System model

We consider a square area of surface ℓ^2. Horizontal and vertical streets are generated within this area using a MPLP of intensities λ_x and λ_y. The LOS links, building penetration and corner diffraction are respectively modeled by means of eq (3.1), eq. (3.4) and eq. (3.7).

We will consider three different tiers for this network :

- The first tier consists of clusters of BSs for every street. In every street, N_{bs} BSs and N_{us} UEs are distributed (by sampling from a uniform law). Each UE is served by N_{aus} antennas. As a result, every BS serves $N_{ubs} = N_{us}/N_{bs}$ users and consists thus of $N_{abs} = N_{ubs}N_{aus}$ transmit antennas. All the BSs in the same street cooperate and form one cluster (in the same manner as in Chapter 4) in order to manage the LOS interference between their associated users;

- The second tier consists of picocells located at N_p street junctions (that are randomly selected among all the crossroads of the MPLP). The role of this second tier is to model locations characterized by a higher density of users (shopping malls, metro stations,etc). Each of these cells is supposed to be centered at its association junction and to stretch up to a distance d_{lim} in every direction. Every junction contains N_{bp} BSs and N_{up} users. These users are served by N_{aup} antennas and each BS serves $N_{ubp} = N_{up}/N_{bp}$ users and thus consists of $N_{abp} = N_{ubp}N_{aup}$ antennas. The BSs of each picocell are clustered as well;

- The last tier consists of N_m macrocells that divide the square ℓ^2 into equal areas. Each macro cell only has one BS located at its center and positioned at the top of a building. Every BS is assumed to have a number of antennas sufficient to serve all of its users. The role of these cells is to serve users that can not be served by the BSs of the other tiers if these BSs are already full in terms of associated users. These macrocell users are distributed

within streets and junctions by means of PPPs of intensities λ_{ms} and λ_{mp}. Each of these users is served by N_{aum} antennas.

An example of such network is displayed in figure 6.1. It is also assumed that all users consist of one receive antenna (independently of their tier) and that they are all affected by a constant noise backgroud σ^2. For each street, picocell or macrocell, the user association policy is the same as section 4.1.2. We assume a Rayleigh fading on every link, as in the previous chapters.

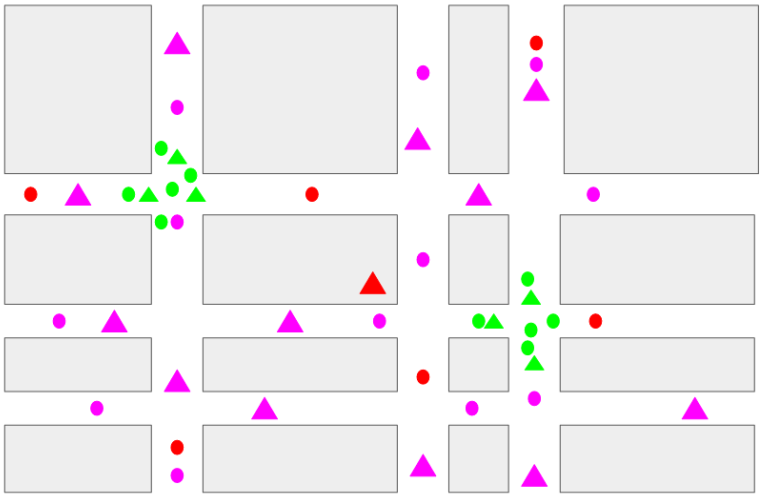

Figure 6.1: Example of node distributions. The red, green and purple colors respectively represent the macrocell, picocell and street nodes. The triangles and circles represent BSs and UEs.

6.2 Numerical results

The network has been simulated for the set of parameters indicated in the table below. ZF beamforming has been used for all transmissions. The resulting coverage for an equal power allocation is displayed in figure 6.2.

ℓ	5.10^3	N_{aus}	1
λ_x	10^{-2}	N_p	8
λ_y	10^{-2}	d_{lim}	50
w_e	-14 dB	N_{bp}	4
w_i	-0.198 dB	N_{up}	50
α_{out}	3	N_{aup}	1
α_{in}	1.7	N_m	4
σ^2	tuned to result in a mean SNR of 25 dB	λ_{ms}	1
N_{bs}	10	λ_{mp}	1
N_{us}	40	N_{aum}	1

The following comments can be made :

- First of all, the coverage of picocell users is significantly high compared to the global network coverage. This is due to the fact that the BSs serving these users are much closer to them compared to the other tiers. Their path loss is hence particularly small;

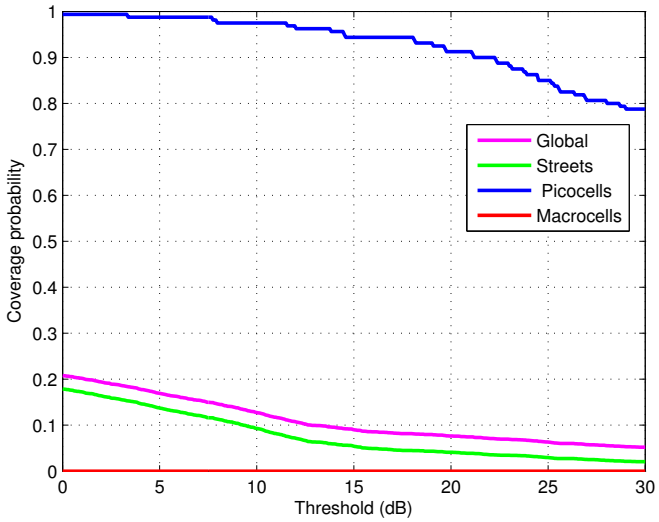

Figure 6.2: Coverage probability the different tiers of the network for equal power allocations.

- By contrast, the coverage of users associated to macrocells is zero above a threshold of 0 dB. Two reasons can be given to justify this observation. On the one hand, the users of macrocells are not orthogonal to most of the users located in the same streets or junctions. They are hence likely to suffer from much LOS interference. On the other hand, it is assumed that the useful power coming from macrocell BSs is attenuated by all the buildings between them. This hypothesis is not completely realistic compared to practical networks. However, considering that the link is only LOS is not entirely true either. A three-dimensional model for the macrocell links (taking into account the height of the buildings) would probably enable to obtain more accurate results.

- Applying the Min-Max algorithm to the network leads to a unique value for all the users. However, this value is below 0 dB on average. Besides, applying this algorithm may not be possible in practice since the tiers do not necessarily coordinate to allocate powers.

As a conclusion, one can add that nothing is done at this stage to manage the interference between tiers, and even between clusters of a same tier. This issue must hence be solved if one wishes to obtain higher coverage values, but this part is left for future work.

Chapter 7

Conclusion

7.1 Summary of contributions

In this master thesis, new SG-based models have been developed in order to encompass important aspects in the design and the optimization of wireless communication networks. First of all, we have tackled the modeling of the propagation environment by extending the work done in [Sh13]. We focused on urban environments represented by Manhattan Poisson line processes. Coverage estimation formulas have been derived taking into account penetration and diffraction losses, as well as variable street and node densities.

Secondly, MIMO networks have been analyzed from an innovative point of view. Several BS distributions and beamforming strategies have been compared under a fixed transmit power constraint. Coverage estimation formulas have been detailed as well. Based on both analytical and simulation results, interpretations have been provided in order to understand the impact of shadowing on the performance of the beamformers.

Then, power control algorithms have been designed and applied to the developed networks. The use of these allocation schemes has enabled to maximize several metrics expressed as objective functions of optimization problems.

Finally, a test case representing a heterogeneous network has been proposed. This test case included elements and methods introduced throughout the thesis. The simulation results highlighted the importance of managing the inter-tier interference.

7.2 Further research directions

7.2.1 Analytical models

It is certainly possible to go further in the development of SG-based formulas. Potential extensions are listed below :

- The expressions derived in Chapter 4 are valid for a fading environment only. It might be possible to develop other expressions accounting for shadowing environments (other than urban grids) with obstacles of various shapes. For example, the content of [Sh19] proposes a model where obstacles are modeled using circles. It may be possible to use a similar approach to model the variable-diameter obstacles of Chapter 4 ;
- The development of new tractable PPs is one of the most important fields of research in stochastic geometry [SG3]. Indeed, modern networks can include nodes with a more specific correlation than in the PPP or the HCPP that are used within this thesis. A potential

extension to this work might be to derive new formulas by means of a PP that would be more representative of the distribution of BSs in actual cities ;

- A comprehensive analysis of the upcoming 5G networks will require to consider three-dimensional effects in order to model massive MIMO arrays more realistically [MIMO22]. Encompassing these effects in the SG framework is likely to be a challenge in terms of complexity (owing to the beamforming and the propagation environment). However, this would probably be an important step in terms of modeling. Up to the author's knowledge, no such contribution has been published so far in the literature.

7.2.2 Heterogeneous networks

General hetnets have not been addressed in this document. The design and analysis of these networks is more complex for several reasons. As mentioned above, strategies must be developed to manage the inter-tier interference. Furthermore, each tier can be modeled by a different PP. This brings a lot of complexity in terms of macroparameters. A direct future contribution might be to model such a K-tier network and find approaches to systematically optimize it as a function of its macroparameters.

7.2.3 Beyond classical models

The content of this thesis has been mostly dedicated to traditional homogeneous MIMO networks. However, the general analysis of networks can cover many other topics that can be more advanced or more exotic. Several possible subjects are listed below. This list must not be seen as an exhaustive enumeration of what can be done in wireless communications but rather as a set of subjects that can interestingly be analyzed in a SG framework.

- Other types of networks can be analyzed such as cognitive networks or relay networks ;
- New wireless technologies can be studied : device-to-device communications (D2D), vehicule-to-vehicule (V2V), full duplex transmissions, etc [SG3] ;
- The global network performance can be characterized using more advanced metrics than the coverage probability or the BER. For instance, secure communications can be assessed in terms of secrecy rate [Misc62]. This metric represents the rate at which information can be transmitted without being revealed to an eavesdropper. In this case, a joint use of SG and random graph theory can be employed within the analysis [SG2] ;
- SG could play a role in the self optimization of networks [SG3]. Indeed, current networks consist of a large number of elements, making it impossible to perform a real time centralized optimization. To solve this issue, SG could be used to find a trade-off between performance and complexity by using the statistical distributions of the network variables (noise, UEs positions, etc).

Publications

The following papers have been written in the framework of this master thesis :

- C. Wiame, L. Vandendorpe and C. Oestges, "Stochastic Geometry Based Coverage Estimation Using Realistic Urban Shadowing Models," Technical Document, *Third Technical Meeting of the COST action CA15104 (IRACON)*, February 2017.

- C. Wiame, L. Vandendorpe and C. Oestges, "Stochastic Geometry-Based Comparison of Network Deployments under a Fixed Transmit Power Constraint", *28th Annual IEEE International Symposium on Personal, Indoor and Mobile Radio Communications (IEEE PIMRC'17)*, October 2017 (submitted for publication in June 2017).

Bibliography

Stochastic geometry

[SG1] J. G. Andrews, A. K. Gupta, H. S. Dhillon, "A Primer on Cellular Network Analysis Using Stochastic Geometry," published on October 5, 2016 on Arxiv.org, <https://arxiv.org/pdf/1604.03183.pdf>, accessed on 4 April 2017.

[SG2] M. Haenggi, J. G. Andrews, F. Baccelli, O. Dousse, and M. Franceschetti, "Stochastic geometry and random graphs for the analysis and design of wireless networks," *IEEE Journal on Selected Areas in Communications*, vol. 27, issue 7, September 2009.

[SG3] H. ElSawy, A. Sultan-Salem, M.-S. Alouini and M. Z. Win, "Modeling and Analysis of Cellular Networks Using Stochastic Geometry : A Tutorial," *IEEE Communications surveys and tutorials*, vol. 19, no. 1, first quarter 2017.

[SG4] H. ElSawy, E. Hossain, and M. Haenggi, "Stochastic Geometry for Modeling, Analysis, and Design of Multi-Tier and Cognitive Cellular Wireless Networks: A Survey," *IEEE Communications surveys and tutorials*, vol. 15, no. 3, third quarter 2013.

[SG5] F. Baccelli and B. Blaszczyszyn, *Stochastic Geometry and Wireless Networks, Volume I -Theory*, B. NoW Publishers, 2009.

[SG6] J. Teichmann, F. Ballani, K.G. Van den Boogaart, "Generalizations of Matérn's hard-core point processes," September 13, 2012, available on Arxiv.org, <https://arxiv.org/pdf/1209.2566.pdf>, accessed on 10 April 2017.

[SG7] T. Lei, X. Wen, Z. Lu, W. Jing, K. Chen and X. Zhao, "A modified Matérn hard core point process for modeling and analysis of dense IEEE 802.11 networks," *International Symposium on Wireless Communication Systems*, 2016.

[SG8] N. Deng, W. Zhou and M. Haenggi, "The Ginibre Point Process as a Model for Wireless Networks with Repulsion," *IEEE Transactions on Wireless Communications*, vol. 14, issue 1, 2015.

[SG9] N. Deng, W. Zhou and M. Haenggi, "The Ginibre Point Process as a Model for Wireless Networks with Repulsion," *IEEE Transactions on Wireless Communications*, vol. 14, issue 1, 2015.

[SG10] M. Di Renzo and W. Lu, "The Equivalent-in-Distribution (EiD)-Based Approach: On the Analysis of Cellular Networks Using Stochastic Geometry," *IEEE Communications Letters*, vol. 18, no. 5, May 2014.

Shadowing models

[Sh11] Y. Jin Chun, S. L. Cotton, H. S. Dhillon, F. Javier Lopez-Martinez, J. F. Paris, and S. Ki Yo, "A Comprehensive Analysis of 5G Heterogeneous Cellular Systems operating over -μ Shadowed Fading Channels," published on 4 October 2016 on Arxiv.org, <https://arxiv.org/abs/1609.09696>, accessed on 6 April 2017.

[Sh12] L. Moreno-Pozas and E. Martos-Naya, "A Random Matrix Model for -μ Shadowed Fading," published on 23 March 2015 on Arxiv.org, <https://pdfs.semanticscholar.org/dd14/978e372e3f01e21c8b2cbd20eb5ae48bf260.pdf>, accessed on 6 April 2017.

[Sh13] F. Baccelli and X. Zhang, "A Correlated Shadowing Model for Urban Wireless Networks," *IEEE Conference on Computer Communication*, 2015.

[Sh14] X. Zhang, F. Baccelli and R. W. Heath, Jr, "An Indoor Correlated Shadowing Model," *IEEE Global Communications Conference*, 2015.

[Sh15] J. Lee, X. Zhang and F. Baccelli, "Shadowing and Coverage in Poisson Buildings," *IEEE INFOCOM 2016 - The 35th Annual IEEE International Conference on Computer Communications*, 2016.

[Sh16] T. Bai, R. Vaze and R. W. Heath, Jr., "Using Random Shape Theory to Model Blockage in Random Cellular Networks," *International Conference on Signal Processing and Communications*, 2012.

[Sh17] A. K. Gupta, J. G. Andrews and Robert W. Heath, Jr., "Macro diversity in Cellular Networks with Random Blockages," published on 9 January 2017 on Arxiv.org, <https://arxiv.org/pdf/1701.02044.pdf>, accessed on 7 April 2017.

[Sh18] T. Bai, R. Vaze and R. W. Heath, "Analysis of Blockage Effects on Urban Cellular Networks," *IEEE Transactions on Wireless Communications*, vol. 13, issue 9, 2014.

[Sh19] K. Venugopal and R. W. Heath, Jr., "Millimeter Wave Networked Wearables in Dense Indoor Environments," *IEEE Access*, vol. 4, pp. 1205 - 1221, 2016.

[Sh20] L. Raschkowski, P. Kyösti, K. Kusume, T. Jämsä, *METIS Channel Models*, ICT-317669-METIS/D1.4, February 2015

[Sh21] J.-E. Berg, "A recursive method for street microcell path loss calculations," In Personal, Indoor and Mobile Radio Communications, PIMRC'95, September 1995.

MIMO networks

[MIMO22] Y. Xie, B. Li, Xiaoya Zuo, M. Yang and Zhongjiang Yan, "A 3D Geometry-based Stochastic Model for 5G Massive MIMO Channels," *11th EIA International Conference on Heterogeneous Networking for Quality, Reliability, Security and Robustness*, 2015.

[MIMO23] N. Seifi, J. Zhang, R. W. Heath, Jr., T. Svensson and M. Coldrey, "Coordinated 3D Beamforming for Interference Management in Cellular Networks," *IEEE Transactions on wireless communications*, vol. 13, no. 10, October 2014.

[MIMO24] F. Baccelli and A. Giovanidis, "A Stochastic Geometry Framework for Analyzing Pairwise-Cooperative Cellular Networks," *IEEE Transactions on wireless communications*, vol. 14, no. 2, February 2014.

[MIMO25] N. Lee and R. W. Heath, Jr., D. Morales-Jimenez and A. Lozano, "Coordinated Beamforming with Dynamic Clustering: A Stochastic Geometry Approach," *IEEE ICC 2014 - Communications Theory*, 2014.

[MIMO26] G. Nigam, P. Minero and M. Haenggi, "Coordinated Multipoint in Heterogeneous Networks: A Stochastic Geometry Approach," *IEEE Transactions on Communications*, vol. 62, issue 11, November 2014.

[MIMO27] S. Akoum and R. W. Heath, Jr., "Multi-cell coordination : A stochastic geometry approach," *IEEE 13th International Workshop on Signal Processing Advances in Wireless Communications*, 2012.

[MIMO28] I. Hwang, C.-B. Chae, J. Lee, Robert W. Heath, Jr., "Multicell cooperative systems with multiple receive antennas," *IEEE Wireless Communications*, February 2013

[MIMO29] A. Shojaeifard, K. Ashour Hamdi, E. Alsusa, D. K. C. So, J. Tang and K.-K. Wong, "Design, Modeling, and Performance Analysis of Multi-Antenna Heterogeneous Cellular Networks," *IEEE Transactions on communications*, vol. 64, vo. 7, July 2016.

[MIMO30] T. Parfait, Y. Kuang and K. Jerry, "Performance Analysis and Comparison of ZF and MRT Based Downlink Massive MIMO Systems," *Sixth International Conference on Ubiquitous and Future Networks*, 2014.

[MIMO31] A. Kamal Hassan, M. Moinuddin and U. M. Al-Saggaf, "Beamforming in Massive MU-MIMO Cellular Networks: A Stochastic Geometry Approach," *6th International Conference on Intelligent and Advanced Systems*, 2016.

[MIMO32] M. G. Khoshkholgh, K. Navaie, K. G. Shin and V. C. M. Leung, "Coverage Performance of MIMO-MRC in Heterogeneous Networks: A Stochastic Geometry Perspective," *IEEE 84th Vehicular Technology Conference*, 2016.

[MIMO33] L. Hesham Afify, H. ElSawy, T. Y. Al-Naffouri and M.-S. Alouini, "Unified Tractable Model for Downlink MIMO Cellular Networks using Stochastic Geometry," *IEEE ICC 2016 - Wireless Communications Symposium*, 2016.

[MIMO34] T. Ba and R. W. Heath, Jr., "Analyzing Uplink SINR and Rate in Massive MIMO Systems Using Stochastic Geometry," *IEEE Transactions on communications*, vol. 64, no. 11, November 2016.

[MIMO35] N. Jindal and A. Lozano, "A unified treatment of optimum pilot overhead in multipath fading channels," *IEEE Transactions on communications*, vol. 58, no. 10, pp. 2939-2948, October 2010.

Power control algorithms

[PC36] C. André Pitz, E. Luiz Ortiz Batista and R. Seara, "On the Joint Beamforming and Power Control in Cellular Systems: Algorithm and Stochastic Model," *IEEE Transactions on wireless communications*, vol. 13, no. 12, December 2014.

[PC37] M. Cui, B.-J. Hu, X. Li and H. Chen, "A Novel Power Control Algorithm for Massive MIMO Cognitive Radio Systems Based on Game Theory," *IEEE 81st Vehicular Technology Conference*, 2015

[PC38] M. Cui, B.-J. Hu, X. Li, H. Chen, S. Hu and Y. Wang, "Energy-Efficient Power Control Algorithms in Massive MIMO Cognitive Radio Networks," *IEEE Access*, vol.5, pp. 1164-1177, 2017.

[PC39] Z. Wang, L. Jiang and C. He, "Optimal Price-Based Power Control Algorithm in Cognitive Radio Networks," *IEEE Transactions on Wireless Communications*, Vol. 13, No. 11, November 2014.

[PC40] M. Chen, F. Liu and Z. Zeng, "Power control algorithm based on the interference statistic properties in heterogeneous networks," *IEEE 26th Annual International Symposium on Personal, Indoor and Mobile Radio Communications*, 2015.

[PC41] M. Chiang, P. Hande, T. Lan and C. Wei Tan, *Power Control in Wireless Cellular Networks*, now Publishers Inc, 2008.

[PC42] P. Siyari and H. Aghaeinia, "Distributed Power Control in Multiuser MIMO Networks with Optimal Linear Precoding," *7th International Symposium on Telecommunications*, 2014.

[PC43] G. Scutari, D. P. Palomar and S. Barbarossa, "The MIMO Iterative Waterfilling Algorithm," *IEEE Transactions on signal processing*, 2009.

[PC44] E. Karipidis, D. Yuan, Q. He and E. G. Larsson, "Max–Min Power Control in Wireless Networks With Successive Interference Cancelation," *IEEE Transactions on wireless communications*, vol. 14, no. 11, November 2015.

[PC45] M. Schubert and H. Boche, "Solution of the Multiuser Downlink Beamforming Problem With Individual SINR Constraints," *IEEE Transactions on vehicular technology*, vol. 53, no. 1, January 2004.

[PC46] M. Chiang, *Networked Life: 20 Questions and Answers*, Cambridge University Press, 2012.

[PC47] Jinho Choi, "Massive MIMO With Joint Power Control," *IEEE Wireless Communication Letters*, vol. 3, No. 4, August 2014.

Heterogeneous networks

[HetNet48] L. Wu, Y. Zhong, W. Zhang and M. Haenggi, "Scalable Transmission Over Heterogeneous Networks: A Stochastic Geometry Analysis," *IEEE Transactions on vehicular technology*, vol. 66, no. 2, February 2017.

[HetNet49] Y. Shen, L. Jiang, C. He, J. Ding and Qi Xi, "Stochastic Geometry Based Cell Load Analysis in Heterogeneous Networks," *IEEE Globecom Workshops*, 2016.

[HetNet50] E. Turgut and M. Cenk Gursoy, "Coverage in Heterogeneous Downlink Millimeter Wave Cellular Networks," *IEEE Transactions on Communications*, vol. PP, issue 99, 2017.

[HetNet51] Y. Wang and Q. Zhu, "Modeling and Analysis of Small Cells Based on Clustered Stochastic Geometry," *IEEE Communication Letters*, vol. 21, no. 3, March 2017.

[HetNet52] H. Wei, N. Deng, W. Zhou and M. Haenggi, "Approximate SIR Analysis in General Heterogeneous Cellular Networks," *IEEE Transactions on Communications*, vol. 64, issue 3, 2016.

Miscellaneous

[Misc53] K. S. Gilhousen, I. Jacobs, R. Padovani, A. J. Viterbi, L. Weaver, and C. Wheatley, "On the capacity of a cellular CDMA system," *IEEE Transaction Vehicular Technology*, vol. 40, no. 2, pp. 303–12, May 1991.

[Misc54] M. S. Alouini and A. J. Goldsmith, "Area spectral efficiency of cellular mobile radio systems," *IEEE Transaction Vehicular Technology*, vol. 48, no. 4, pp. 1047–66, July 1999.

[Misc55] M. Elmenouar, "By 2020 - 5G will Deliver 50 Gbps Peak Data Rate," published on September 9, 2015, on Linkedin.com <https://www.linkedin.com/pulse/2020-5g-deliver-6-gbps-commercial-peak-data-rate-50-elmenouar>, accessed on 4 April 2017.

[Misc56] C. Wiame, L. Vandendorpe and C. Oestges, "Stochastic Geometry Based Coverage Estimation Using Realistic Urban Shadowing Models," *IRACON Cost Action, 3rd technical meeting*, January 2017.

[Misc57] S. M. Ross *Introduction to Probability Models*, 9th edition, Boston: Academic Press, 2007.

[Misc58] S. Asmussen, J. Ledet Jensen, L. Rojas-Nandayapa, "On the Laplace Transform of the Lognormal Distribution," *Methodology and Computing in Applied Probability*, vol. 18, issue 2, pp 441–458, June 2016.

[Misc59] Wireless nets, http://www.wireless-nets.com/resources/tutorials/define_SNR _values.html, accessed on 25 May 2017.

[Misc60] Digi knowledge base, http://knowledge.digi.com/articles/Knowledge_Base /Understanding-LTE-Signal-Strength-Values, accessed on 6 June 2017.

[Misc61] ELKI Data mining framework,
https://elki-project.github.io/tutorial/same-size _k _means, accessed on 14 April 2017.

[Misc62] A. Rabbachin, A. Conti and Moe Z. Win, "Wireless Network Intrinsic Secrecy," *IEEE/ACM Transactions on Networking*, vol. 23, no. 1, 2015.

[Misc63] C. Oestges and L. Vandendorpe, "LELEC2796 - Wireless communications : mobile propagation channels," Ecole polytechnique de Louvain, Université catholique de Louvain, 2016.

[Misc64] C. Oestges and A. J. Paulraj, "Propagation Into Buildings for Broad-Band Wireless Access," IEEE transactions on vehicular technology, vol. 53, no. 2, March 2004.

[Misc65] C. Wiame, L. Vandendorpe and C. Oestges, "Stochastic Geometry-Based Comparison of Network Deployments under a Fixed Transmit Power Constraint", *28th Annual IEEE International Symposium on Personal, Indoor and Mobile Radio Communications (IEEE PIMRC'17)*, October 2017 (submitted for publication in June 2017).

[Misc66] D. Arthur and S. Vassilvitskii, "k-means++ : The Advantages of Careful Seeding," Stanford,
http://ilpubs.stanford.edu:8090/778/1/2006-13.pdf, accessed on 22 May 2017

Rue Archimède, 1 bte L6.11.01, 1348 Louvain-la-Neuve **www.uclouvain.be/epl**